

Physical Properties of Weak MgII Absorbers at $z \sim 2$ ¹

Ryan S. Lynch

*Department of Astronomy, P.O Box 400325, University of Virginia, Charlottesville, VA
22904*

rsl4v@virginia.edu

and

Jane C. Charlton

*Department of Astronomy and Astrophysics, The Pennsylvania State University,
University Park, PA 16802*

charlton@astro.psu.edu

ABSTRACT

We present the results of photoionization modeling of nine weak MgII ($W_r < 0.3 \text{ \AA}$) quasar absorption line systems with redshifts $1.4 < z < 2.4$ obtained with the Ultraviolet and Visual Echelle Spectrograph on the Very Large Telescope. These systems have been chosen because they provide access to a regime of red-shift space that previous weak MgII studies have not looked at. The densities, metallicities, Doppler parameters, and column densities of these systems are compared to those of other weak MgII systems at lower redshift. There is no significant statistical variation in the properties of the absorbers over the redshift range $0.4 < z < 2.4$. The number density per unit redshift is known to decrease for weak MgII absorbers between $z \sim 1$ and $z \sim 2$ by a greater amount than predicted from cosmological effects and changes in the extragalactic ionizing background alone. We suggest that, because the physical properties of the absorber population are not seen to change significantly across this range, that the evolution in dN/dz is due to a decrease in the activity that gives rise to weak MgII absorption, and not due to a change in the processes that form weak MgII absorbers. The presence of separate, but aligned (in velocity) low and high density clouds in all single cloud weak MgII absorbers provides an important diagnostic of their geometry. We discuss possible origins in dwarf galaxies and in extragalactic analogs to high velocity clouds.

¹Based on public data obtained from the ESO archive of observations from the UVES spectrograph at the VLT, Paranal, Chile. ESO Program ID 166.A-0106. HE2217-2818 observed during UVES commissioning.

Subject headings: intergalactic medium—quasars: absorption lines

1. Introduction

Weak MgII absorbers are defined to be those with rest frame equivalent widths $W_r < 0.3 \text{ \AA}$ and represent a different population than strong MgII absorbers (Rigby et al. 2002; Nestor et al. 2005). Strong MgII absorbers are known to be associated with luminous galaxies (within $\sim 38h^{-1}(L/L^*)^{0.15}$ kpc) (Bergeron & Boissé 1991; Bergeron et al. 1992; Le Brun et al. 1993; Steidel et al. 1994, 1997; Steidel 1995), while weak MgII absorbers are not typically seen within a $50h^{-1}$ kpc impact parameter of a luminous galaxy (Rigby et al. 2002, but see Churchill et al. (2005) for some exceptions). The exact environment(s) and process/processes that give rise to weak MgII absorbers is not yet known, but they may arise in dwarf galaxy environments, in the cosmic web surrounding galaxies, and/or in high velocity clouds. Weak MgII absorbers generally correspond to sub-Lyman limit systems ($15.8 < \log N(\text{HI}) < 16.8[\text{cm}^{-2}]$) (Churchill et al. 1999b; Rigby et al. 2002; Churchill et al. 2000) and they have metallicities of at least 10% solar and as high as solar or even supersolar (Rigby et al. 2002; Charlton et al. 2003; Simcoe et al. 2006). In addition, the FeII/MgII ratio of some absorbers does not allow for α -enhancement, thus Type Ia supernovae must contribute as well as Type II. Because Type Ia supernovae cannot eject metals to large distances, metals must be produced “*in situ*”.

The number statistics and kinematics of single cloud weak MgII absorbers lend themselves best to a flattened geometry and suggest that the absorbers may be produced by higher density regions in the cosmic web (Milutinović et al. 2005). MgII absorption typically arises in a high density region $\sim 1\text{--}100$ pcs thick which is often surrounded by a lower density region that gives rise to high ionization CIV absorption centered at the same velocity as the MgII (Charlton et al. 2003; Simcoe et al. 2006). Additional low density regions producing CIV absorption, that are detected at different velocities than MgII, often exist.

While most weak MgII absorbers can be fit by a single Voigt profile component, about one third have multiple components (Churchill et al. 2000; Lynch et al. 2006). Some of these multiple cloud weak MgII absorbers are weaker versions of strong MgII absorbers with similar kinematics, as if they arise in the outskirts or in sparse regions of luminous galaxies. Others, which tend to have more kinematically compact profiles, have been hypothesized to arise in dwarf galaxies (Zonak et al. 2004; Ding et al. 2005; Masiero et al. 2005).

When exploring the nature of weak MgII absorbers, two methods are often used—statistical surveys and photoionization modeling of individual systems. Narayanan et al.

(2005), Churchill et al. (1999b), and Lynch et al. (2006) conducted surveys of systems with equivalent widths in the range $0.02 \leq W_r \leq 0.3 \text{ \AA}$, which when combined, span the redshift range $0 < z < 2.4$. These surveys obtained number densities of absorbers per unit redshift (dN/dz): $dN/dz = 1.00 \pm 0.20$ ($0 < z < 0.3$) (Narayanan et al. 2005), $dN/dz = 1.74 \pm 0.10$ ($0.4 < z < 1.4$) (Churchill et al. 1999b), and $dN/dz = 1.06 \pm 0.12$ ($1.4 < z < 2.4$) (Lynch et al. 2006). Apparently, the population of weak MgII absorbers peaks at $z \sim 1$ over the range $0 < z < 2.4$. Furthermore, the density of absorbers at $z \sim 2$ is significantly lower than expected if the change in dN/dz was due only to cosmological effects and to the changing extragalactic background radiation (Lynch et al. 2006). This indicates that either the same process creates weak MgII absorbers across this redshift range but was less active at $z \sim 2$ than at $z \sim 1$, or that the physical mechanisms responsible for creating the absorbers change across redshift and are more efficient at $z \sim 1$ than at $z \sim 2$. It should be noted that this trend in dN/dz is consistent with the star formation history in dwarf galaxies (Gabasch et al. 2004; Kauffmann et al. 2004), which may suggest that weak MgII absorbers are related to this activity.

Photoionization models facilitate the exploration of the physical properties of the absorption system, such as ionization parameter, density, temperature, abundance pattern, and size. By understanding these properties for absorbers at different redshifts, we can gain insight into what processes create them. If different processes are responsible for the formation of these absorbers at different epochs, then the physical properties of the absorbers are likely to evolve. If no statistical difference in the physical properties is observed, this would suggest that the same mechanism is responsible for creating weak MgII absorbers at different epochs. To this end, we have produced photoionization models of the nine $1.4 < z < 2.4$ systems found by Lynch et al. (2006) using the code Cloudy (Ferland et al. 1998) and compared our results to those of systems at lower redshift (Rigby et al. 2002; Charlton et al. 2003; Zonak et al. 2004; Ding et al. 2005; Masiero et al. 2005). Our methodology for modeling the systems is the subject of § 2. In § 3 we report the results of our models for each individual system. In § 4 we discuss our results and their implications for the population of weak MgII absorbers and end with a conclusion in § 5.

2. Modeling Methodology

The 9 systems selected for modeling were taken from Lynch et al. (2006), and were identified through a detection of a weak MgII $\lambda\lambda 2796, 2803$ doublet in the redshift range $1.4 < z < 2.4$. The systems were chosen because they lie in a region of redshift-space ($1.4 < z < 2.4$) that previous weak MgII studies have not looked at. In order to be accepted

as a true detection, the MgII $\lambda\lambda 2796, 2803$ had to be detected at at least a 5σ significance level in MgII $\lambda 2796$. For a detailed discussion of the data reduction procedure see Kim et al. (2004), and for a discussion of the survey method see Lynch et al. (2006). Once an absorption system was identified, the Doppler parameter and column density of the MgII $\lambda\lambda 2796, 2803$ doublet were measured from a Voigt profile fit to the doublet using Minfit (Churchill et al. 2003). This code finds the minimum number of components required for an adequate fit to the observed absorption of MgII.

The measured MgII column density was used as a direct constraint for the photoionization code Cloudy 94.00 last described by Ferland et al. (1998) (i.e. the photoionization models were “optimized” on the column density of MgII). For each cloud (separate Voigt profile component) a grid was constructed for which the metallicity ($\log Z/Z_{\odot}$) and ionization parameter ($\log U = \log n_e/n_{\gamma}$) were changed in incremental values, typically in steps of 0.5 dex. A solar abundance pattern was assumed unless otherwise noted. A Haardt & Madau ionizing background of quasars plus star forming galaxies with a photon escape fraction of 0.1 for $z < 3$, was used at the redshift of each system (Haardt & Madau 1996, 2001). This radiation was assumed to be incident on a plane parallel slab. Cloudy calculated column densities for all detected transitions and an equilibrium temperature for the cloud. This temperature was used along with the measured Doppler parameter of MgII to calculate the turbulent/bulk motion contribution to the total Doppler parameter, $b_{turb}^2 = b_{tot}^2 - 2kT/m_{Mg}$. This b_{turb} was then applied to calculate the expected b_{tot} for every other element, again using the equilibrium temperature given by Cloudy. The model column densities and Doppler parameters of all clouds were used to generate a synthetic spectrum which was convolved with the instrumental profile appropriate for UVES, $R = 45,000$. These were compared to the data by using χ^2 indicators combined with profile inspection in order to refine the metallicity and ionization parameter values of the model. At times, it was necessary to adjust the abundance pattern of the model in order to achieve an adequate fit to the observed spectrum. The effect of such changes on model parameters is given in the individual system descriptions. We assume a solar abundance pattern unless otherwise stated.

Many of the low wavelength transitions fell in the Ly α forest and contained significant blends. In this case, a model was taken to be acceptable if it did not overproduce the observed absorption of a given transition. However, when blends were not present, a more exact match was required. In some cases a range of model parameters produced an adequate fit. In the case of blends, an upper or lower limit was often the only constraint that could be obtained.

In most cases, there was absorption in higher ionization transitions that Cloudy could not reproduced through the low ionization MgII phase (i.e. the clouds that were optimized on

the MgII column density). This happened either because the high ionization absorption was too broad to arise from the low ionization phase, or because the high ionization absorption was not sufficiently produced for ionization parameters that provided a sufficient fit to low and intermediate ionization absorption. In these cases, the Doppler parameters and column densities of the CIV $\lambda\lambda 1548, 1550$ doublet were measured using Mifit and Cloudy models were produced, optimizing on CIV. The combined low and high ionization phase models were compared to the data. Separate constraints on metallicity and ionization parameter were obtained for the high ionization clouds, when possible. However, it is common that the low ionization phase has only a lower limit on metallicity in order not to overproduce Ly α absorption. For higher values of metallicity, an additional contribution to Ly α from the high ionization phase would be required. In the event that there was a blend in the expected location of the CIV $\lambda\lambda 1548, 1550$ doublet, the SiIV $\lambda\lambda 1393, 1402$ doublet was used instead. If there were blends in the expected locations of both these transitions, no constraint on the high ionization phase could be obtained (though this was a problem for only the $z = 1.708494$ system toward HE0151-4326).

In addition to a Haardt & Madau ionizing background of quasars plus star forming galaxies with a photon escape fraction of 0.1 for $z < 3$, the effect of using an ionizing background including only quasars was also explored. In most cases, this change had little effect, and the small effect it did have was only seen in the high ionization gas. The sole exception is the $z = 1.450109$ absorber towards Q0122-380, for which the effect of the change of spectral shape is described in § 3.3.

3. Properties of Individual Systems

The results of the photoionization modeling of our nine systems are presented here and a summary can be found in Table 1. Voigt profile fit results with errors obtained using Mifit are presented in Table 2. The best-fit models are superimposed on key constraint transitions in Figures 1–9.

3.1. HE2347-4342 $z = 1.405362$

This is a single cloud weak MgII absorber, i.e. there is only one resolved component of absorption in MgII. A second phase is required to reproduce the observed CIV absorption. The ionization parameter is constrained to be $-3.0 \leq \log U \leq -2.5$ for the MgII phase and $\log U \geq -1.8$ for the CIV phase. Higher values for the ionization parameter in the low phase

give rise to an overproduction of SiIV and AlIII, and lower values fail to produce enough AlIII. A lower ionization parameter in the high phase overproduces SiIV. Using a number density of photons of $\log n_\gamma = -4.83$ at this redshift (Haardt & Madau 2001), this corresponds to $-2.3 \leq \log n_H \leq -1.8$ [cm^{-3}] for the MgII phase and $\log n_H \leq -3.1$ [cm^{-3}] for the CIV phase. This constraint is based upon a solar ratio of Fe to Mg. However, higher densities would apply if there is α -enhancement (i.e. if the Fe to Mg ratio is lower than the solar value). Ly α is not covered due to the low redshift of this system, so there is no constraint on metallicity. In the optically thin regime, our constraints on $\log U$ are insensitive to the assumed metallicity.

3.2. Q0002-422 $z = 1.446496$

This is a single cloud absorber in MgII. A second phase is required to reproduce the observed CIV absorption. The ionization parameter is constrained to be $-3.5 \leq \log U \leq -3.0$ for the low ionization phase, and $-1.8 \leq \log U \leq 1.3$ for the high ionization phase. Lower ionization parameters for the low phase overproduce OI, and higher values overproduce SiIV. The constraint on the high phase is based upon the strength of the SiIV $\lambda\lambda 1393, 1402$ doublet. Using a $\log n_\gamma = -4.82$, we find $-1.8 \leq \log n_H \leq -1.3$ [cm^{-3}] for the MgII phase and $-3.5 \leq \log n_H < -3.0$ [cm^{-3}] for the CIV phase. For an α -enhanced model, lower densities would apply. Ly α is not covered due to the low redshift of this system, so there is no constraint on metallicity.

3.3. Q0122-380 $z = 1.450109$

This is a multiple cloud absorber in MgII with three resolved components, and requires a second phase to reproduce the observed CIV absorption. The ionization parameter is constrained to be $-4.0 \leq \log U \leq -2.5$ for the MgII phase across all clouds, and $-1.8 \leq \log U \leq -1.7$ for the CIV phase. Higher values of the ionization parameter for the low phase overproduce AlIII, and lower values overproduce OI. A different ionization parameter for the high phase does not reproduce the observed SiIV absorption. Using a number density of photons of $\log n_\gamma = 4.82$, we find $-2.3 \leq \log n_H \leq -0.8$ [cm^{-3}] for the MgII phase and $-3.2 \leq \log n_H \leq -3.0$ for the CIV phase. Ly α is not covered due to the low redshift of this system, so there is no constraint on metallicity.

For this system, a change of the ionizing spectrum from “quasar plus star-forming galaxies” to “quasar-only” (see § 2) did have a non-negligible effect. In the “quasar-only”

case, the ionization parameter in the high ionization phase needed to be increased by 0.3 dex to $\log U \sim -1.5$, and the abundance of aluminum needed to be decreased by 0.5 dex relative to solar.

3.4. HE2217-2818 $z = 1.555845$

This is a multiple cloud absorber in MgII with six resolved components, and requires a second phase to reproduce the observed CIV absorption. The ionization parameter is constrained to be $\log U = -4.0$ for the MgII phase, and $-2.5 \leq \log U \leq -2.0$ in the CIV phase. A high ionization parameter for the low phase overproduces AlIII while a lower ionization parameter under-produces the observed FeII absorption. Other values of the ionization parameter for the high phase cannot reproduce the observed SiIV absorption. Using a number density of photons of $\log n_\gamma = -4.78$, we find $\log n_H \leq -0.8$ [cm^{-3}] for the MgII phase and $-2.8 \leq \log n_H \leq -2.3$ [cm^{-3}] for the CIV phase. It is likely that α -enhancement is required to explain the observed absorption of Fe and Al within this range of ionization parameters. The strength of the Ly α line, relative to the low ionization transitions, implies a metallicity of $\log Z/Z_\odot \geq -1.4$.

3.5. HE0001-2340 $z = 1.651462$

This is a narrow, single cloud absorber in MgII. Two phases are needed to reproduce the observed CIV absorption. There are two possibilities for fitting the low ionization phase. One is to use $\log U \geq -3.5$ and to decrease the abundances of Si, Al, and C relative to the solar value. The other possibility is to use $\log U \leq -4.0$ and to decrease the abundances of Fe, Al, and C relative to solar. The magnitude of the required adjustment is only about 0.7 dex for each element. Using a number density of photons of $\log n_\gamma = -4.8$, we find $\log n_H \leq -1.3$ [cm^{-3}] and $\log n_H \geq -0.8$ [cm^{-3}], respectively, for the two values of ionization parameter. The higher ionization parameter decreases the observed Fe absorption but overproduces the Si absorption, while the lower ionization parameter decreases the observed Si absorption but overproduces the Fe absorption. We remark that these abundance patterns are consistent with dust depletion and that this is one possible explanation for the observed absorption profiles (Welty et al. 2002). The ionization parameter is constrained to be $-1.7 \leq \log U \leq -1.5$ for the CIV phase based upon the observed SiIV $\lambda\lambda 1393, 1402$ doublet, corresponding to $-3.25 \leq \log n_H \leq -3.05$ [cm^{-3}]. The strength of the Ly α line implies a metallicity of $\log Z/Z_\odot \geq -1.5$ for the low ionization phase. For the CIV phase, low metallicities ($\log Z/Z_\odot = -2.5$ for the blueward component and $\log Z/Z_\odot = -1.7$ for the

redward component) fit the Ly α profile, but higher metallicities and a separate Ly α phase are also permitted.

3.6. HE0151-4326 $z = 1.708494$

This is a single cloud absorber in MgII. Due to blends at the expected locations of the CIV $\lambda\lambda 1548, 1550$ doublet and the SiIV $\lambda\lambda 1393, 1402$ doublet, it is not possible to absolutely determine if a second, high ionization phase is needed. The ionization parameter for the low ionization phase is constrained to be $\log U \geq -4.0$, which is based upon the observed strength of FeII absorption. Using a number density of photons of $\log n_\gamma = -4.74$, we find $\log n_H \leq -0.7$ [cm $^{-3}$]. For the high phase, if used, we find an ionization parameter of $\log U = -2.3$. This corresponds to $\log n_H = -2.4$. A metallicity of $\log Z/Z_\odot \geq -1.5$ is required in order not to overproduce Ly α in the red wing, however, the blue wing of Ly α requires a separate, extremely low metallicity phase to be fit.

3.7. HE2347-4342 $z = 1.796237$

This is a very weak, narrow single cloud absorber in MgII, though a very weak second component improves the fit in the blue wing. Due to blends at the expected locations of the CIV $\lambda\lambda 1548, 1550$ doublet and the SiIV $\lambda\lambda 1393, 1402$ doublet, there is some ambiguity in our assessment of a second phase. However, because the SiIV and CIV are weak, for some parameter choices it is possible for them to arise in the same phase with the MgII. There are two possibilities for modeling the MgII phase. First, we can use an ionization parameter of $\log U \geq -3.2$ to match the observed FeII but decrease the abundance of Si and Al relative to the Solar value to fit the observed SiII and AlII. Alternatively, we can match the observed abundance of SiIII by using an ionization parameter $-4.0 \leq \log U \leq -3.2$ but decrease the abundance of Si, Al, and Fe. Using a number density of photons of $\log n_\gamma = -4.72$, we find $\log n_H \leq -1.5$ [cm $^{-3}$] or $-1.5 \leq \log n_H \leq -0.7$ [cm $^{-3}$], respectively. If a second phase is used to fit the high ionization transitions, the parameters are $-2.0 \leq \log U \leq -1.0$, so as not to overproduce SiIV. This corresponds to $-2.7 \leq \log n_H \leq -3.7$. The metallicity of the low ionization phase is constrained to be $\log Z/Z_\odot \geq -1.0$. However, the observed Ly α absorption can not be fully matched without using a separate, extremely low metallicity phase, even with the addition of the broader high ionization phase.

3.8. Q0453-423 $z = 1.858380$

This is a multiple cloud absorber in MgII with six resolved components. A second phase is needed to fit SiIII and SiIV $\lambda 1403$. Though CIV is badly blended, we know that it is relatively weak, classifying this as a CIV deficient system. The ionization parameter of the low ionization phase is constrained to be $\log U = -4.0$ in order to produce the observed FeII absorption. Using a number density of photons of $\log n_\gamma = -4.71$, we find $\log n_H = -0.8$ [cm^{-3}]. This model does not produce the observed SiIII or SiIV and it does not produce significant CIV absorption. A second phase with $\log U = -2.8$ can account for the observed SiIII and SiIV but slightly overproduces MgII, SiII, and CIV. A slight (few tenths of a dex) abundance pattern adjustment of these elements could resolve this discrepancy. The strength of the Ly α line implies a metallicity of $\log Z/Z_\odot \geq -2.0$ for the low ionization phase, but additional offset high ionization components, not constrained by these data, could contribute substantially to the Ly α absorption. If so, the low ionization phase could have substantially higher metallicity.

3.9. HE0940-1050 $z = 2.174546$

This is a single cloud absorber in MgII. A second phase is required to reproduce the observed CIV absorption. The ionization parameter is constrained to be $\log U \geq -2.5$ for the MgII phase, and $-2.0 \leq \log U \leq -1.0$ for the five clouds in the CIV phase. The bluest cloud in the CIV phase has the lowest ionization parameter. A higher ionization parameter in the low phase will overproduce high ionization transitions, however, lower ionization parameters require a reduction in the abundance of aluminum and iron by up to 0.7 dex. The ionization parameter in the high phase is constrained by the observed absorption of SiIV. Using a number density of photons of $\log n_\gamma = -4.69$, we find $\log n_H \leq -2.2$ [cm^{-3}] for the MgII phase and $-3.7 \leq \log n_H \leq -2.7$ [cm^{-3}] for the five clouds in the CIV phase. The strength of the Ly α line implies a metallicity of $\log Z/Z_\odot \geq -2.0$. Another phase is required to match the blue wing of the Ly α profile.

4. Discussion

We have compared the basic and derived properties of weak MgII absorbers over the redshift range $0.4 < z < 2.4$. We include the 9 systems at $1.4 < z < 2.4$ from the survey of Lynch et al. (2006) as well as systems from Rigby et al. (2002); Charlton et al. (2003); Zonak et al. (2004); Ding et al. (2005); Masiero et al. (2005) with $z < 1.4$. We consider

single and multiple cloud weak MgII absorbers separately, since they are likely to have different origins.

One of the most important basic properties of single cloud weak MgII absorbers at $0.4 < z < 1.4$ is their two phase structure. MgII is found to arise in a higher density region, while the strength of the CIV absorption requires a separate, lower density region (Rigby et al. 2002). This same two phase structure is also found in all four single cloud weak MgII absorbers at $1.4 < z < 2.4$ for which it was possible to place a constraint on a second phase. The other two single cloud weak MgII absorbers in the $1.4 < z < 2.4$ sample had blends at the expected location of CIV that prevented us from deriving a constraint. For comparison, the weaker extragalactic background radiation (EBR) at $z \sim 0$ would lead to broader MgII components arising from the high ionization phase of single cloud weak MgII absorbers, and to detectable MgII absorption from some structures that at higher redshift produced only high ionization absorption (Narayanan et al. 2005).

Most $0.4 < z < 1.4$ multiple cloud weak MgII absorbers also require separate phases to explain simultaneously the observed MgII and CIV absorption. Our three multiple cloud weak MgII absorbers at $1.4 < z < 2.4$ also required two phase models. At both redshift regimes, we see examples of CIV-deficient multiple cloud weak MgII absorbers, where a second phase may not be needed (e.g., the $z = 0.5584$ system toward PG1241 + 176 (Ding et al. 2005) and the $z = 0.7290$ system toward PG1248 + 401 (Masiero et al. 2005)) or is needed, but produces only weak absorption (our $z = 1.796237$ system toward HE2347-4342).

Thus there may be a difference between single and multiple cloud weak MgII absorbers in the fraction that have a second, lower density phase producing relatively significant CIV absorption. Also, there seems to be a significant difference in the nature of the second phase in cases where it is required. For single cloud weak MgII absorbers, both at $0.4 < z < 1.4$ and at $1.4 < z < 2.4$, there is always a CIV cloud centered on the MgII (within $\sim 3 \text{ km s}^{-1}$). There may also be additional, offset CIV clouds, which tend to be weaker. The multiple cloud weak MgII absorbers do not usually have a direct correspondence between the CIV and the MgII clouds. In both types of absorbers, we might postulate a sheetlike or shell geometry, with separate layers responsible for the MgII and CIV absorption. However, in the case of the single cloud MgII absorbers it would appear that the layers are quite quiescent, and are moving in unison. This would suggest an origin in an environment that has not experienced recent star formation or turbulence.

Figure 10 shows MgII column density vs. z for single cloud systems, and Figure 11 shows their Doppler parameter vs. z . There is no apparent change in these parameters across redshift. The same can be said for Figures 12 and 13, which show column density vs. z and Doppler parameter vs. z for multiple cloud systems, respectively. Table 2 also gives

this information.

Figure 14 shows $\log n_H$ vs. z for systems with a single absorption component in MgII. There is a large spread in the derived properties for the low redshift absorbers, but no systematic trend is apparent across redshift. In most cases, only upper limits could be obtained for the density. However, limits for $\log n_H$ of the high redshift systems are consistent with those of the low redshift systems. To verify that there is no significant evolution, we applied the Spearman-Kendall nonparametric rank correlation tests, which take into account the upper limits in the data (Isobe, Feigelson, & Nelson 1986; LaValley, Isobe, & Feigelson 1992). The Spearman and Kendall tests showed 62% and 85% chances that a correlation is not present.

Figure 15 shows $\log n_H$ vs. z for multiple cloud absorbers. Although our sample size is small, again there is no obvious change in the properties of the absorbers across redshift. Figure 16 shows $\log Z/Z_\odot$ vs. z for single cloud absorbers. Metallicity constraints could not be obtained for all absorbers because there was not always coverage of the Ly α line. Taking into account the limits, we cannot see a significant change in the properties with redshift. The Spearman-Kendall tests yielded a large probability (0.80 and 0.33) that there is no correlation. However, it is worth noting that we do yet know of a $z > 1.4$ absorber with a high (close to solar) metallicity. There are a few solar or higher metallicity absorbers (25% of the sample) at $z < 1.4$. Figure 17 shows $\log Z/Z_\odot$ vs. z for multiple cloud absorbers. Once again, we suffer from a small sample size, but the metallicities of the high redshift systems are consistent with those of the low redshift systems.

First, we consider the possible implications of our results on the multiple-cloud absorbers. This class can be broadly grouped into two categories. First, there are those multiple cloud absorbers that are “kinematically spread” and are likely to be “almost-strong” MgII absorbers for which the line-of-sight simply does not pass through dense regions of gas. Second, there are those multiple cloud absorbers that are “kinematically compact” and are likely dwarf galaxies or are associated with dwarf galaxies (Zonak et al. 2004; Ding et al. 2005; Masiero et al. 2005). The $z = 1.450109$ system toward Q0122-380 is an example of a kinematically compact absorber. The metallicity of this system is constrained to be $-1.0 \leq \log Z/Z_\odot \leq 0.0$. The $z = 1.555845$ system towards HE2217-2818 and the $z = 1.858380$ system toward Q0453-423 are examples of kinematically spread absorbers. The metallicities of these two systems are constrained to be $\log Z/Z_\odot \geq -1.1$ and $\log Z/Z_\odot \geq -2.0$. Because the metallicities of our systems are not well constrained, we cannot draw any definite conclusions about the environments in which each type of system arises.

The redshift path density of single cloud weak MgII absorbers is observed to decrease

between $z \sim 1$ and $z \sim 2$ (Churchill et al. 1999b; Lynch et al. 2006). Some of this evolution is due to the changing EBR which ranges from $-4.83 < \log n_\gamma < -4.71$ [cm^{-3}] between $1.4 < z < 2.4$, respectively. The effect of the changing EBR is to lead to more low ionization MgII gas at lower redshift. In addition, cosmological effects will lead to a decrease in the density of weak MgII absorbers at lower redshift. When these two competing effects are taken together, they cannot fully account for the lower dN/dz at $z \sim 2$. The range of physical conditions that were found in this study (column density, Doppler parameter, density, and metallicity) for systems at redshift $1.4 < z < 2.4$ do not show a statistical variation from systems at redshift $0.4 < z < 1.4$. The ranges are large, constraints are derived using different transitions at different redshifts, and our samples are small, leading to dilution of any trends. However, at face-value our result is consistent with the idea that the evolution in the weak MgII absorber population from $z \sim 2$ to $z \sim 1$ is due to an increase in the efficiency of the mechanisms that create weak MgII absorbers, and not due to a change in the actual mechanisms. For example, if a collapse process gave rise to weak MgII absorbing structures, then, to first order, one would expect a constant range of densities across redshift. Since we see such a constant range, the observed evolution in dN/dz would then be attributed to a change in the number of structures undergoing such a collapse as a function of redshift.

We now turn our attention to the effects of a changing metallicity. As metallicity generally increases with decreasing redshift, we would expect that, at low redshift, lower total hydrogen column density absorbers could give rise to weak MgII absorption. This would lead to a rise in the number of weak MgII absorbers. In our data set, although there is no statistically significant trend, an increase in metallicity with decreasing redshift is still consistent with the data. Because we have a relatively small data set and only have limits in most cases, we cannot draw a firm conclusion on the change in metallicity across redshift. Thus it is possible that the increase in weak MgII absorbers at lower redshift is at least in part due to a systematic increase in metallicity. This may be a fruitful avenue for future study. To improve metallicity constraints, we would need access to lower Lyman series lines. The narrow, low ionization components have a dominant contribution to these Lyman series lines, while the $\text{Ly}\alpha$ absorption can have contributions from broader components (Churchill et al. 1999a, see Figure 4 therein).

In summary, through our modeling we have found that the properties of single cloud weak MgII absorbers at $1.4 < z < 2.4$ are similar to those of single cloud weak MgII absorbers at $0.4 < z < 1.4$. These properties include the existence of two phases, the gas densities, the Doppler parameters, the relatively high metallicities, and the presence of offset CIV components. It is striking that the dominant CIV component, although produced in a different phase, is centered at the same velocity as the MgII cloud. Using the facts that almost all CIV absorbers are found within ~ 100 kpc of luminous galaxies and that half of

CIV absorbers have weak MgII absorption, Milutinović et al. (2005) argued that weak MgII absorbers are likely to arise ~ 50 -100 kpc from luminous galaxies.

Of course, the fundamental goal of our study is to identify single cloud weak MgII absorbers with a specific environment and physical process. The lack of evolution in their properties suggests a common mechanism working over time. The various possibilities include shells or supernova remnants in dwarf galaxies, high velocity clouds, and shells of enriched material surrounding galaxies in the cosmic web. These possibilities have in common the feature that the high and low ionization gas could be separated, but moving at the same velocity, consistent with the arguments of (Milutinović et al. 2005).

Lynch et al. (2006) note that the star formation history in dwarf galaxies seems to be consistent with the evolution of the absorber population, and suggest that this is a possible process that could give rise to weak MgII absorbers. The fact that there is no significant change in the properties of the population across redshift suggest that this scenario is possible. We note that if this idea is correct, then star formation in the regions would have stopped long ago. No UV photons would be left, and so we are justified in using a background spectrum rather than local stellar sources. The results of the present study are consistent with the dwarf galaxy hypothesis.

The origin of single cloud weak MgII absorbers in the extragalactic analogs of high velocity clouds also remains a possibility. The appeal of this scenario is consistency with the phase structure found in Milky Way high velocity clouds (Ganguly et al. 2005; Fox et al. 2005), the similar velocities between low and high ionization gas in the high velocity clouds, and the large covering factor of the sky by Milky Way OVI high velocity clouds (Sembach et al. 2003). If Milky Way high velocity clouds are produced by cool/warm clouds sweeping through the Galactic corona, a similar phenomenon would be expected to occur around other galaxies, leading to typical impact parameters of ~ 50 -100 kpc for lines of sight that pass through the high velocity cloud, but not through the luminous galaxy disk. Any distinction between these sheetlike high velocity clouds structures and portions of the cosmic web clustered near galaxies may just be a matter of semantics. Comparisons between the OVI absorption in single cloud weak MgII absorbers and in Milky Way high velocity clouds is a useful diagnostic, though challenging because of the location of OVI in the Ly α forest.

5. Conclusion

We used the photoionization code Cloudy to model nine weak MgII absorption systems found by Lynch et al. (2006). The Doppler parameter and column density of MgII were mea-

sured using the Mifit program (Churchill et al. 1999b), and these were used as constraints by Cloudy. The ionization parameter and metallicity were then adjusted incrementally in Cloudy for each MgII cloud until the simulated absorption profiles matched the observed absorption profiles of other transitions in the spectra. It was usually necessary to include a second, high ionization phase in order to reproduce the observed absorption in CIV. This was necessary because the CIV profile was too broad and/or too strong to arise solely from the MgII phase gas. It was sometimes the case that only an upper or lower limit could be placed on the conditions of the system due to blends at the expected locations of certain transitions. These results were then compared to models of absorbers at $0.4 < z < 1.4$ and checked for any evolution across redshift.

- 6/9 systems had only a single component of absorption in MgII (single cloud) and the remaining three showed multiple components (multiple cloud)
- A multiphase structure was required in 7/9 systems. One system had blends at the expected location of CIV and SiIV and no definite conclusions about a multiphase structure could be reached. In another system, the CIV profile was weak enough that a second phase was not definitely needed, though it was preferred.
- For single cloud systems we find the following constraints on physical properties:

For the $z = 1.405362$ absorber towards HE2347-4342, $-2.3 \leq \log n_H \leq -1.8$ [cm^{-3}] for the low ionization phase and $\log n_H \leq -3.1$ [cm^{-3}] for the required high ionization phase; No metallicity constraint.

For the $z = 1.446496$ absorber towards Q0002-422, $-1.8 \leq \log n_H \leq -1.3$ [cm^{-3}] for the low ionization phase and $-3.5 \leq \log n_H \leq -3.0$ [cm^{-3}] for the required high ionization phase; No metallicity constraint.

For the $z = 1.651462$ absorber towards HE0001-2340, there are two possibilities for fitting the low ionization phase: $\log n_H \leq -1.3$ [cm^{-3}] with decreases to Si, Al, and C relative to solar, or $\log n_H \leq -0.8$ [cm^{-3}] with decreases to Fe, Al, and C relative to solar; $-3.3 \leq \log n_H \leq -3.1$ [cm^{-3}] for the required high ionization phase; $\log Z/Z_\odot \geq -1.5$.

For the $z = 1.708494$ absorber towards HE0151-4326, $\log n_H \leq -0.7$ [cm^{-3}] for the low ionization phase; Blends in high ionization transitions, but high ionization phase may not be required; $\log Z/Z_\odot \geq -1.5$ for the low ionization phase.

For the $z = 1.796237$ absorber towards HE2347-4342 there are two possibilities for fitting the low ionization phase: $\log n_H \leq -1.5$ [cm^{-3}] or $-1.5 \leq \log n_H \leq -0.7$ [cm^{-3}];

$\log Z/Z_\odot \geq -1.0$ for the low ionization phase; Blends in high ionization phase; weak CIV could arise in same phase with MgII, but separate phase is also permitted.

For the $z = 2.174546$ absorber towards HE0940-1050, $\log n_H \leq -2.2$ [cm^{-3}] for the low ionization phase and $-3.7 \leq \log n_H \leq -2.7$ [cm^{-3}] for the high ionization phase; $\log Z/Z_\odot \geq -2.0$.

- for multiple cloud systems we find the following constraints on physical properties:

For the $z = 1.450109$ absorber towards Q0122-380, $-2.3 \leq \log n_H \leq -0.8$ [cm^{-3}] for the low ionization phase and $-3.2 \leq \log n_H \leq -3.0$ [cm^{-3}] for the high ionization phase; $-1.0 \leq \log Z/Z_\odot \leq 0.0$

For the $z = 1.555845$ absorber towards HE2217-2818, $\log n_H \leq -0.8$ [cm^{-3}] for the low ionization phase and $-2.8 \leq \log n_H \leq -2.3$ [cm^{-3}] for the high ionization phase; $\log Z/Z_\odot \geq 1.1$

For the $z = 1.858380$ absorber towards Q0453-423, $\log n_H \leq -0.8$ [cm^{-3}] for the low ionization phase and $\log n_H = -1.9$ [cm^{-3}] for the high phase; $\log Z/Z_\odot \geq -2.0$

The properties of the absorber population as stated above are not significantly different across the redshift range $0.4 < z < 2.4$, i.e. the variation in parameters over the sample of absorbers that produce weak MgII absorption is larger than any systematic evolution with redshift. These properties include the presence of two phases to produce MgII and CIV absorption and the density of the gas that produces MgII absorption. With a limited number of metallicity constraints at high redshift, the data are consistent either with constant metallicity from $0.4 < z < 2.4$, or with a metallicity that increases with time. With our increased sample size, one of the most significant results is that a required high ionization cloud is always centered within 3 km s^{-1} of the single cloud weak MgII absorption.

The lack of evolution in the properties of single cloud weak MgII absorbers implies that the change in the number statistics of absorbers across redshift is due to changes in the rate of relevant processes and not due to a change in the nature of these processes that give rise to weak MgII absorbers. Another possibility for explaining the evolution of the number of weak MgII absorbers is a systematic increase in metallicity of the absorbing structures from $z \sim 2$ to $z \sim 1$. The close correspondence in the velocities of the low and high ionization phases suggests a layered structure which physically could be consistent with supernova remnants or winds in dwarf galaxies, or with extragalactic analogs to high velocity clouds.

REFERENCES

- Bauer, A. E., Drory, N., Hill, G. J., & Feulner, G. 2005, *ApJ*, 621, L89
- Bergeron, J., & Boissé, P. 1991, *A&A*, 243, 344
- Bergeron, J., Cristiani, S., & Shaver, P. A. 1992, *A&A*, 257, 417
- Charlton, J. C., Ding, J., Zonak, S. G., Churchill, C. W., Bond, N. A., & Rigby, J. R. 2003, *ApJ*, 589, 111
- Churchill, C. W., Kacprzak, G. G., & Steidel, C. C. 2005, *ArXiv Astrophysics e-prints*, arXiv:astro-ph/0504392
- Churchill, C. W., Mellon, R. R., Charlton, J. C., Jannuzi, B. T., Kirhakos, S., Steidel, C. C., & Schneider, D. P. 2000, *ApJ*, 543, 577
- Churchill, C. W., Charlton, J. C. 1999, *AJ*, 118, 59
- Churchill, C. W., Rigby, J. R., Charlton, J. C., & Vogt, S. S. 1999, *ApJS*, 120, 51
- Churchill, C. W., & Vogt, S. S. 2001, *AJ*, 122, 679
- Churchill, C. W., Vogt, S. S., & Charlton, J. C. 2003, *AJ*, 125, 98
- Ding, J., Charlton, J. C., & Churchill, C. W. 2005, *ApJ*, 621, 615
- Ferland, G., Korista, K. T., Verner, D. A., Ferguson, J. W., Kingdon, J. B., & Verner, E. M. 1998, *PASP*, 110, 76
- Fox, A. J., Wakker, B. P., Savage, B. D., Tripp, T. M., Sembach, K. R., & Bland-Hawthorn, J. 2005, *ApJ*, 630, 332
- Gabasch, A., et al. 2004, *ApJ*, 616, L83
- Ganguly, R., Sembach, K. R., Tripp, T. M., & Savage, B. D. 2005, *ApJS*, 157, 251
- Haardt, F., & Madau, P. 1996, *ApJ*, 461, 20
- Haardt, F., & Madau, P. 2001, in *Clusters of Galaxies and the High Redshift Universe Observed in X-rays*, ed. D. M. Neumann & J. T. T. Van (Paris: Recontres de Moriond XXXVI), in press (astro-ph/0106018)
- Isobe, T., Feigelson, E. D., & Nelson, P. I. 1986, *ApJ*, 306, 490

- Kauffmann, G., White, S. D. M., Heckman, T. M., Ménard, B., Brinchmann, J., Charlot, S., Tremonti, C., & Brinkmann, J. 2004, *MNRAS*, 353, 713
- Kim, T.-S., Viel, M., Haehnelt, M. G., Carswell, R. F., & Cristiani, S. 2004, *MNRAS*, 347, 355
- Kim, T.-S., Carswell, R. F., Cristiani, S., DÓdorico, S., Giallongo, E. 2002, *MNRAS*, 335, 555
- Lanzetta, K. M., Wolfe, A. M., & Turnshek, D. A. 1987, *ApJ*, 322, 739
- LaValley, M., Isobe, T., & Feigelson, E. 1992, in *ASP Conf. Ser. 25, Astronomical Data Analysis Software and Systems I*, ed. D. M. Worrall, C. Biemesderger, & J. Barnes (San Francisco: ASP), 245
- Le Brun, V., Bergeron, J., Boisse, P., & Christian, C. 1993, *A&A*, 279, 33
- Lynch, R. S., Charlton, J. C., & Kim, T.-S. 2006, *ApJ*, 640, 81
- Masiero, J. R., Charlton, J. C., Ding, J., Churchill, C. W., & Kacprzak, G. 2005, *ApJ*, 623, 57
- Milutinović, N., Rigby, J. R., Ding, J., Masiero, J. R., Palma, C., & Charlton, J. C. 2005, in preparation
- Narayanan, A., Charlton, J. C., Masiero J. R. & Lynch, R. 2005, submitted
- Nestor, D. B., Turnshek, D. A., & Rao, S. M. 2005, *ApJ*, 628, 637
- Rigby, J. R., Charlton, J. C., & Churchill, C. W. 2002, *ApJ*, 565, 743
- Sembach, K. R., et al. 2003, *ApJS*, 146, 165
- Simcoe, R. A., Sargent, W. L. W., Rauch, M., & Becker, G. 2006, *ApJ*, 637, 648
- Steidel, C. C. 1995, *QSO Absorption Lines*, Proceedings of the ESO Workshop Held at Garching, Germany, 21 - 24 November 1994, edited by Georges Meylan. Springer-Verlag Berlin Heidelberg New York. Also *ESO Astrophysics Symposia*, 1995., p.139, 139
- Steidel, C. C., Dickinson, M., Meyer, D. M., Adelberger, K. L., & Sembach, K. R. 1997, *ApJ*, 480, 568
- Steidel, C. C., Dickinson, M., & Persson, S. E. 1994, *ApJ*, 437, L75

Steidel, C. C., & Sargent, W. L. W. 1992, *ApJS*, 80, 1

Welty, D. E., Jenkins, E. B., Raymond, J. C., Mallouris, C., & York, D. G. 2002, *ApJ*, 579, 304

Weymann, R. J., et al. 1998, *ApJ*, 506, 1

Zonak, S. G., Charlton, J. C., Ding, J., & Churchill, C. W. 2004, *ApJ*, 606, 196

Table 1. Ionization Parameters and Metallicities of $1.4 < z < 2.4$ Weak MgII Systems

QSO	$z_{abs}/\text{Velocity (km s}^{-1}\text{)}$	$\log U$	$\log Z/Z_{\odot}$
HE2347-4342	1.405362	MgII Phase: -3.0 – -2.5 CIV Phase: ≥ -1.8	Ly α not covered
Q0002-422	1.446496	MgII Phase: -3.5 – -3.0 CIV Phase: -1.8 – -1.3	Ly α not covered
Q0122-380	1.450109	MgII Phase: -4.0 – -2.5 CIV Phase: -1.8 – -1.7	Ly α not covered
HE2217-2818	1.555845	MgII Phase: -4.0 CIV Phase: -2.5 – -2.0	≥ -1.4
HE0001-2340	1.651462	MgII Phase: -4.0 – -3.5* CIV Phase: -1.7 – -1.5	≥ -1.5
HE0151-4326	1.708494	MgII Phase: ≥ -4.0 CIV Phase: -2.3	≥ -1.5
HE2347-4342	1.796237	MgII Phase: $\geq -4.0^*$ CIV Phase: -2.0 – -1.0	≥ -1.0
Q0453-423	1.858380	MgII Phase: -4.0 CIV Phase: -2.8	≥ -2.0
HE0940-1050	2.174546	MgII Phase: -3.7 – -2.5 CIV Phase: -2.0 – -1.0	≥ -2.0

Note. — *A more detailed description of these systems can be found in § 3.5 and § 3.7

Table 2. Doppler Parameters and Column Densities of $1.4 < z < 2.4$ Weak MgII Systems

QSO	$z_{abs}/\text{Velocity (km s}^{-1}\text{)}$	$\log N(\text{MgII}) [\text{cm}^{-2}]$	$b \text{ (km s}^{-1}\text{)}$
HE2347-4342	1.405362	11.87 ± 0.01	7.42 ± 0.06
Q0002-422	1.446496	12.09 ± 0.01	6.00 ± 0.06
Q0122-380	1.450109		
Cloud 1	-18.0	11.68 ± 0.08	5.11 ± 0.95
Cloud 2	-3.9	11.59 ± 0.11	8.65 ± 2.52
Cloud 3	40.4	11.76 ± 0.03	10.90 ± 0.89
HE2217-2818	1.555845		
Cloud 1	-79.7	11.38 ± 0.01	6.40 ± 0.02
Cloud 2	-49.2	12.56 ± 0.01	2.69 ± 0.02
Cloud 3	-30.9	11.82 ± 0.01	1.51 ± 0.06
Cloud 4	-14.7	12.02 ± 0.01	8.05 ± 0.10
Cloud 5	4.9	12.62 ± 0.01	5.09 ± 0.02
Cloud 6	37.4	12.16 ± 0.01	3.73 ± 0.03
HE0001-2340	1.651462	12.56 ± 0.01	2.89 ± 0.03
HE0151-4326	1.708494	11.86 ± 0.01	3.90 ± 0.14
HE2347-4342	1.796237	13.26 ± 0.02	4.20 ± 0.07
Q0453-423	1.858380		
Cloud 1	-26.3	11.24 ± 0.04	9.63 ± 1.18
Cloud 2	-1.3	13.05 ± 0.01	6.32 ± 0.02
Cloud 3	23.1	11.40 ± 0.02	5.09 ± 0.41
Cloud 4	50.6	11.98 ± 0.01	13.92 ± 0.32
Cloud 5	100.8	11.80 ± 0.01	1.54 ± 0.28
Cloud 6	125.1	11.93 ± 0.03	$33.83 \pm 2.42^*$
HE0940-1050	2.174546	11.91 ± 0.01	4.64 ± 0.20

Note. — *A defect in the spectrum, most likely a sky line that was not properly removed, is responsible for this anomalous measurement

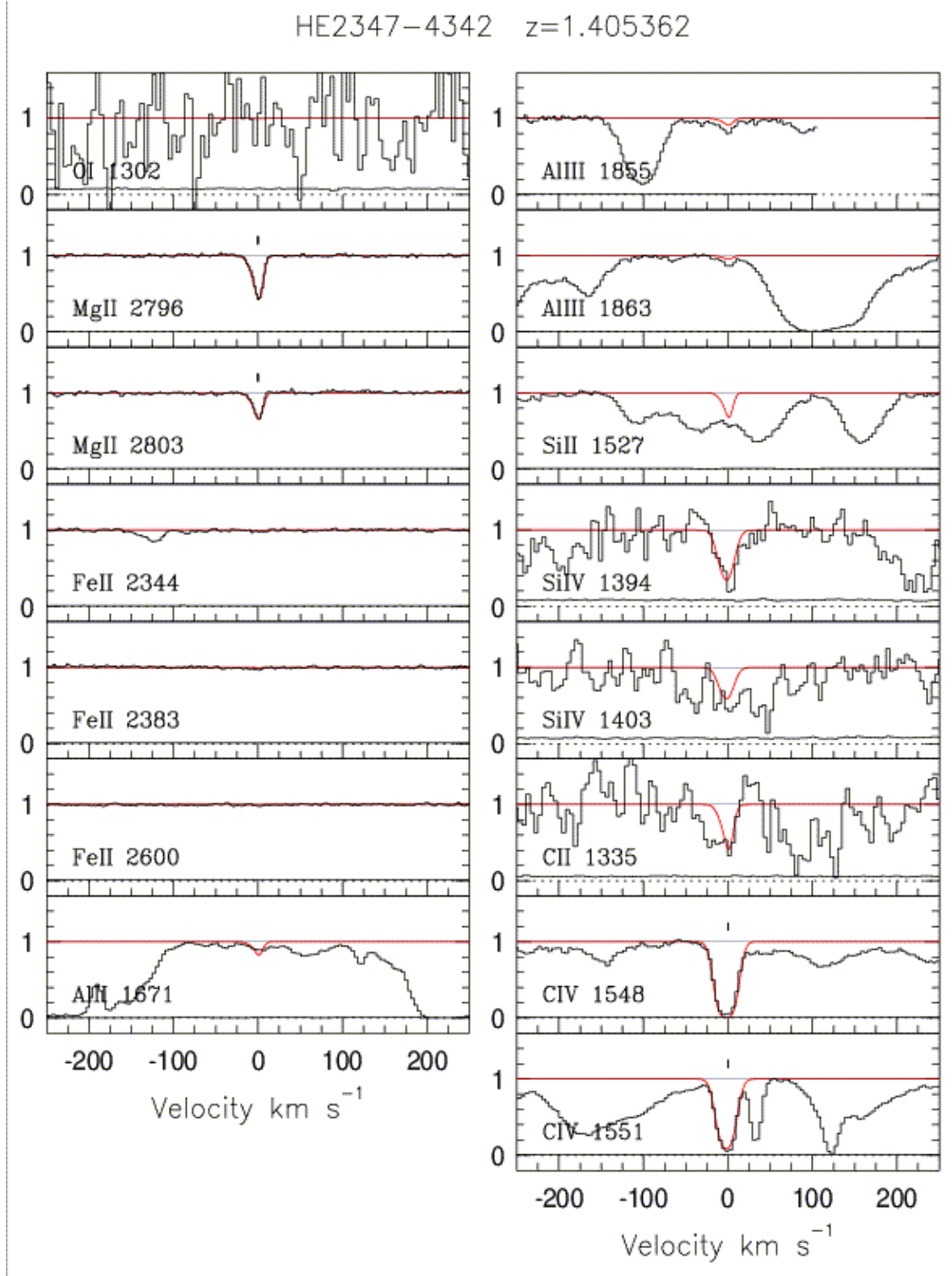


Fig. 1.— The $z = 1.405362$ system towards HE2347-4342. Only relevant transitions are displayed here, in velocity space, centered at the redshift corresponding to the optical depth weighted mean of the $\text{MgII } \lambda 2796$ profile. The error array is plotted, but in some cases is so small that it is difficult to distinguish from zero flux. This model uses $\log U = -3.0$ for the low ionization phase and $\log U = -1.7$ for the high ionization phase, and $\log Z/Z_{\odot} = 0.0$ for both phases. The positions of model clouds from the low ionization phase are marked with ticks on the MgII panels, while the high ionization phase clouds are marked with ticks on the CIV panels. The feature to the right of

Q0002-422 $z=1.446496$

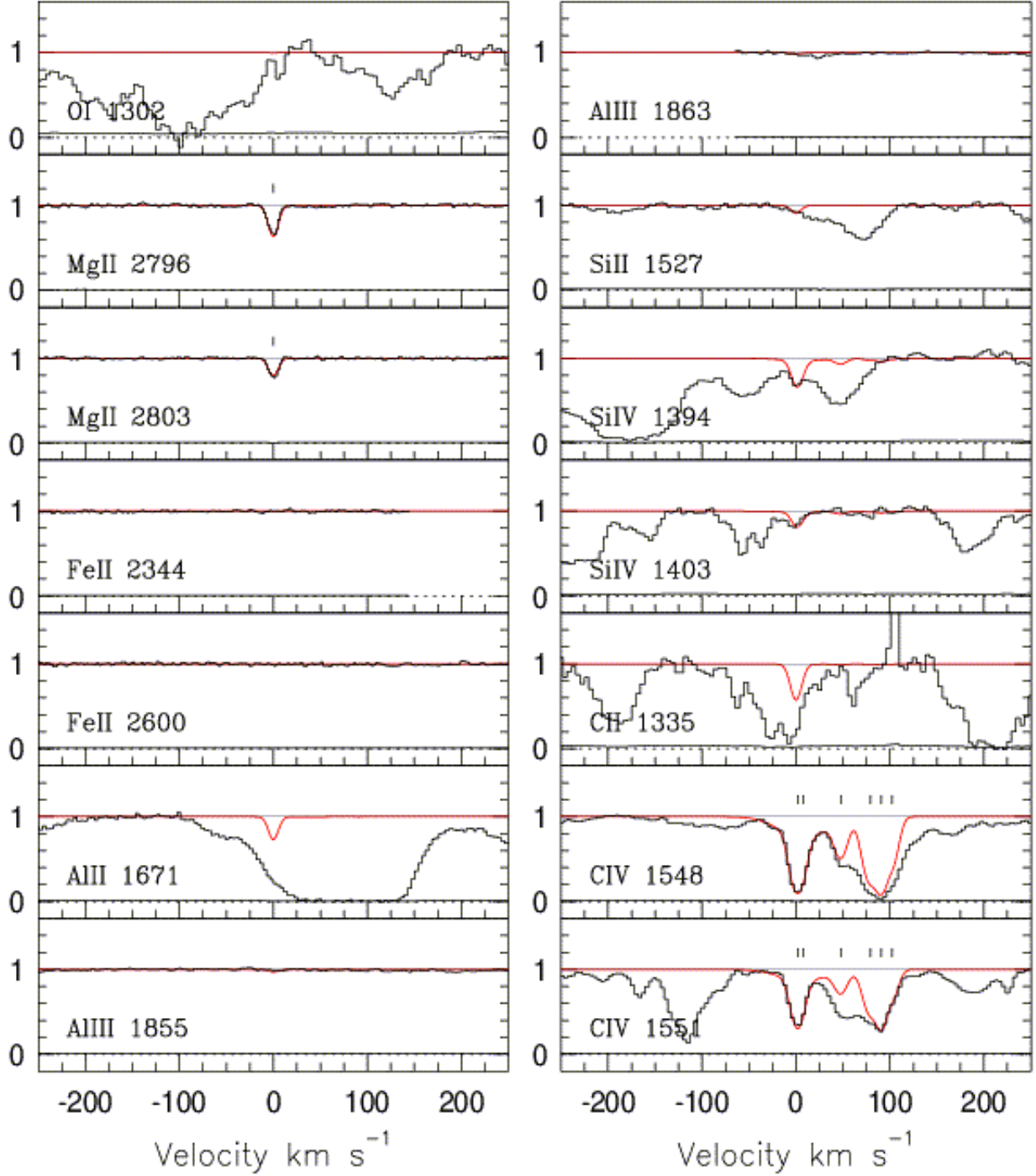


Fig. 2.— The $z = 1.446496$ system towards Q0002-422, displayed as in Fig. 1. Only relevant transitions are displayed here. This model uses $\log U = -3.0$ for the low ionization phase and $\log U = -1.3$ for the high ionization phase. Metallicity is $\log Z/Z_{\odot} = -1.0$

Q 0122-380 $z=1.450109$

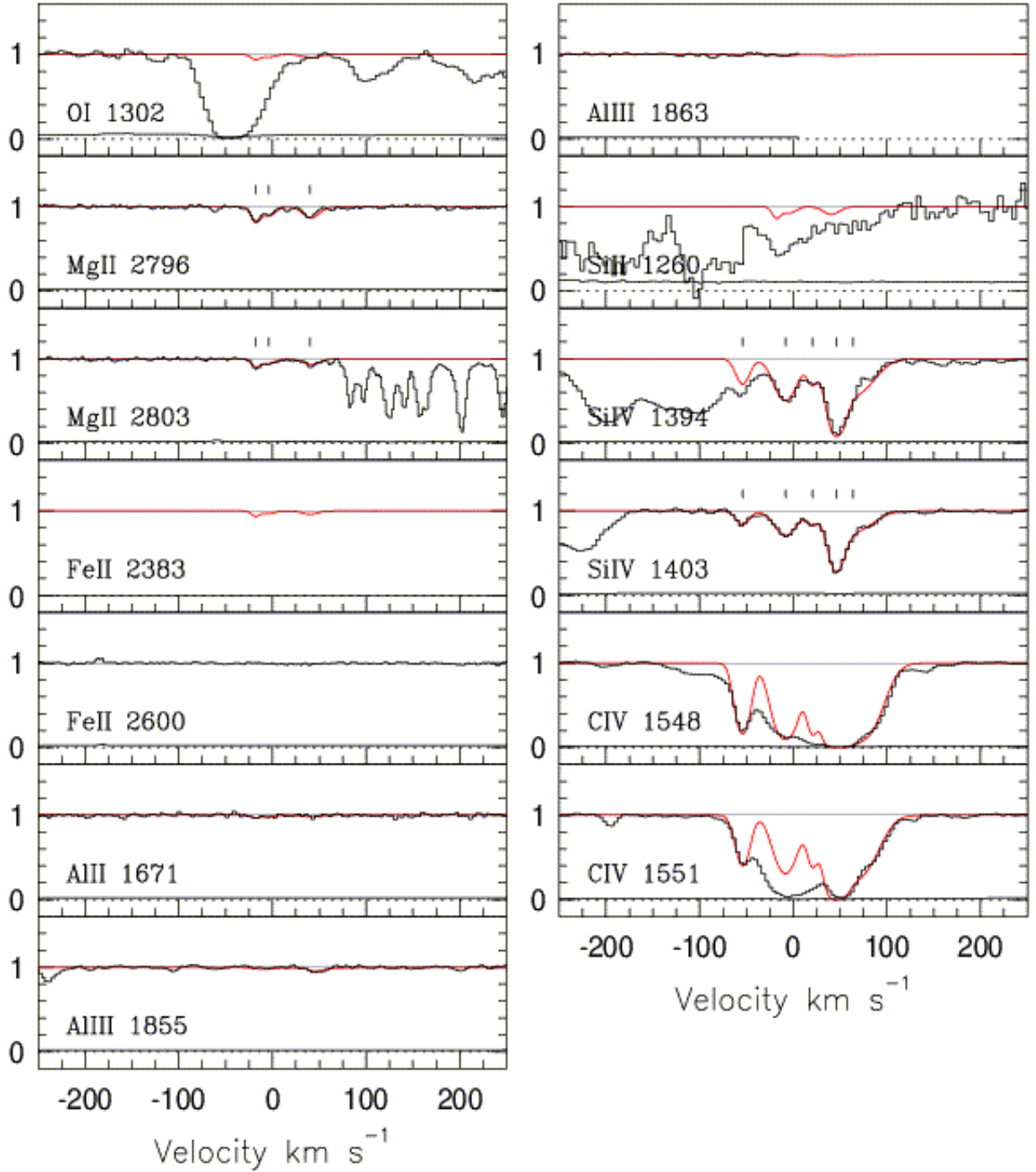


Fig. 3.— The $z = 1.450109$ system towards Q0122-380, displayed as in Fig. 1. Only relevant transitions are displayed here. This model uses $\log U = -5.0$ for the low ionization phase and $\log U = -1.1$ for the high ionization phase. Metallicity is $\log Z/Z_{\odot} = 0.0$ for the low ionization phase and $\log Z/Z_{\odot} = 1.0$ for the high ionization phase.

HE 2217-2818 $z=1.555845$

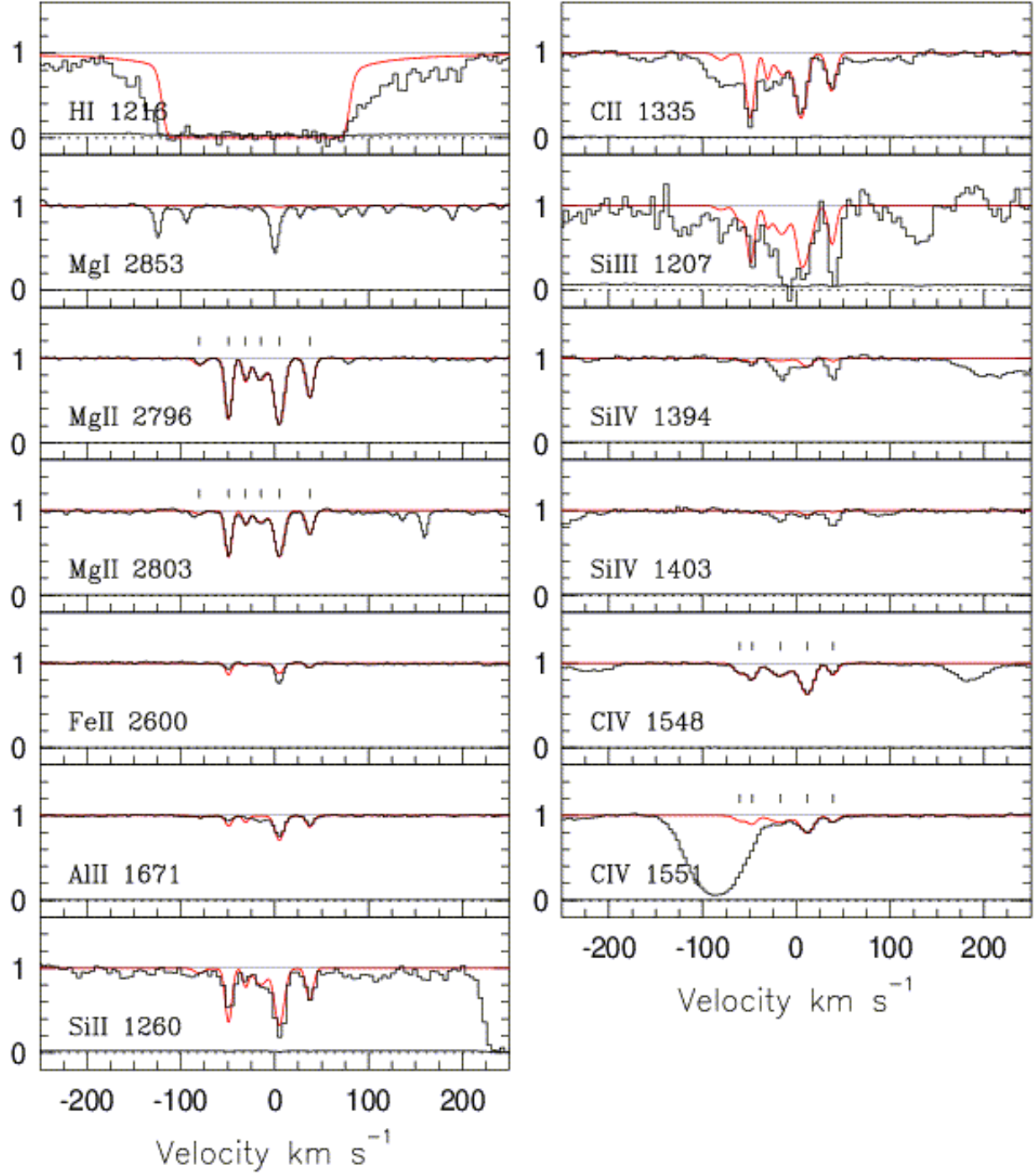


Fig. 4.— The $z = 1.555845$ system towards HE2217-2818, displayed as in Fig. 1. Only relevant transitions are displayed here. This model uses $\log U = -4.0$ for the low ionization phase and $\log U = -2.0$ for the high ionization phase. Metallicity $\log Z/Z_{\odot} = 1.4$

HE 0001–2340 $z=1.651462$

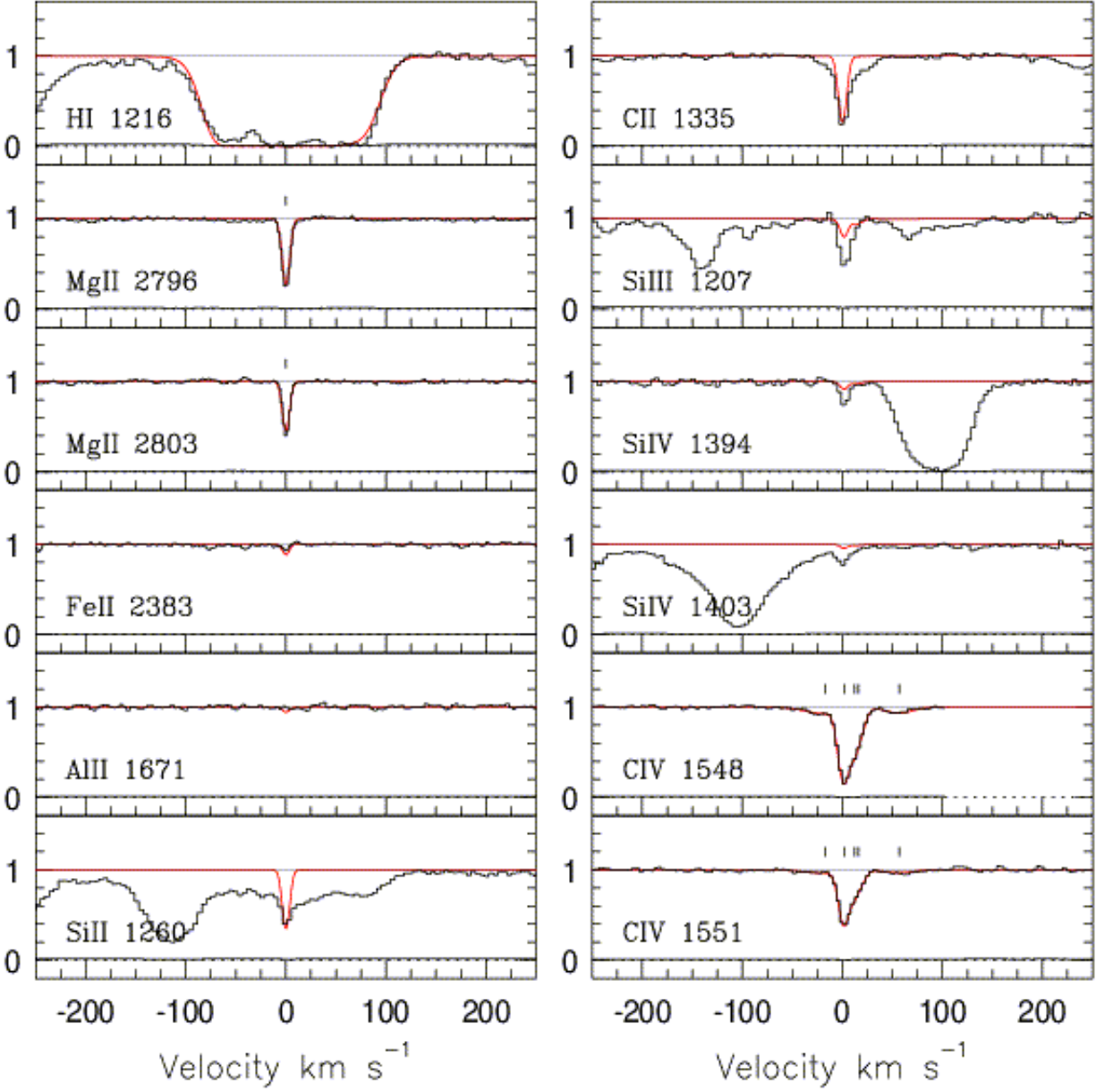


Fig. 5.— The $z = 1.651462$ system towards HE0001-2340, displayed as in Fig. 1. Only relevant transitions are displayed here. This model uses $\log U = -5.0$ for the low ionization phase and $\log U = 0.0$ for the high ionization phase. Metallicity is $\log Z/Z_{\odot} = -1.5$. The abundances of Fe, Al, and C have been lowered relative to solar.

HE 0151–4342 $z=1.708494$

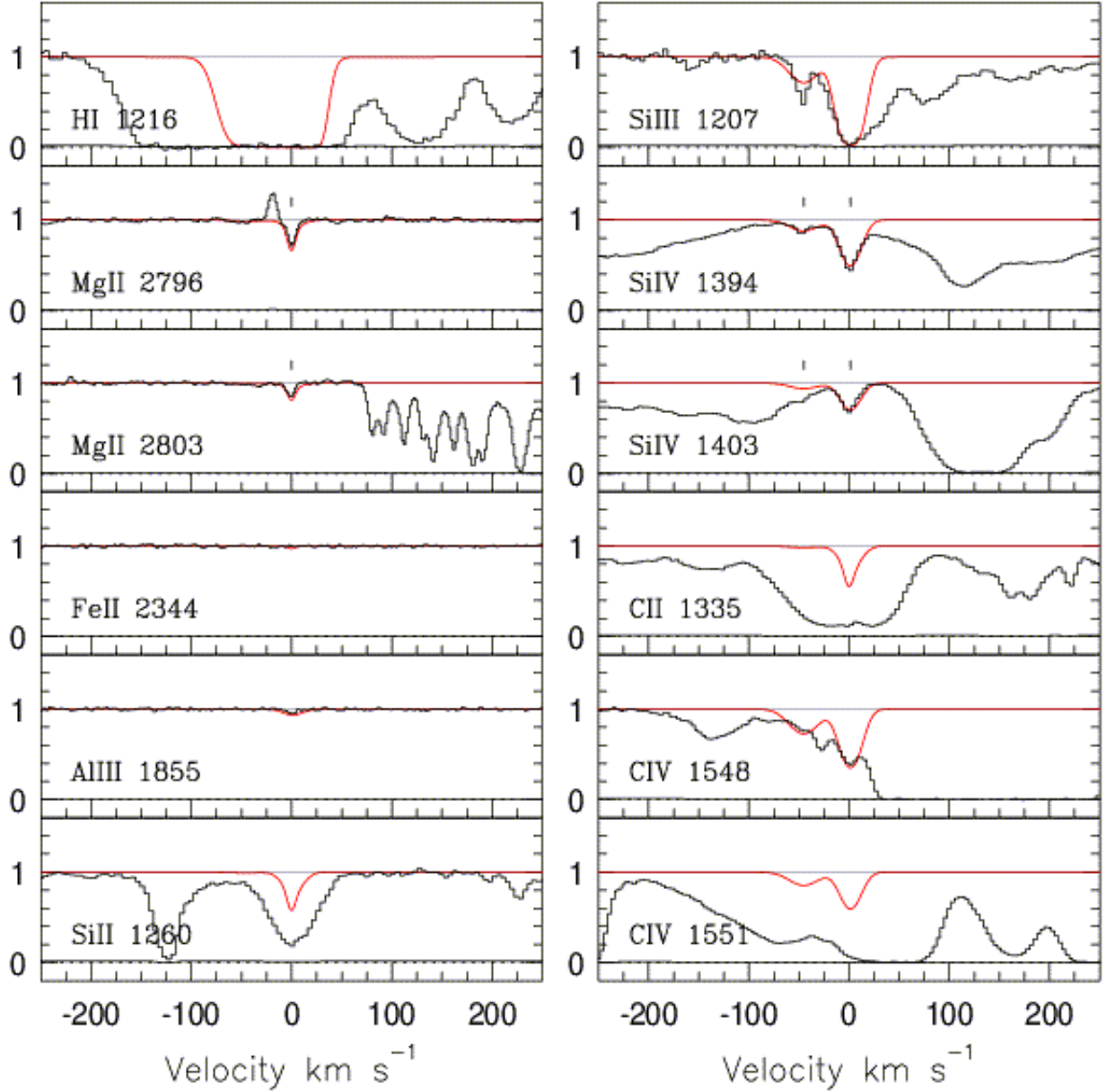


Fig. 6.— The $z = 1.708494$ system towards HE0151-4326, displayed as in Fig. 1. Only relevant transitions are displayed here. This model uses $\log U = -4.0$ for the low ionization phase. The high ionization phase is not required but here we use it with $\log U = -2.0$. Metallicity is $\log Z/Z_{\odot} = -1.0$. The feature to the left of MgII $\lambda 2796$ is an artifact of poor sky subtraction. It has been accounted for in our measurements.

HE 2347–4342 $z=1.796237$

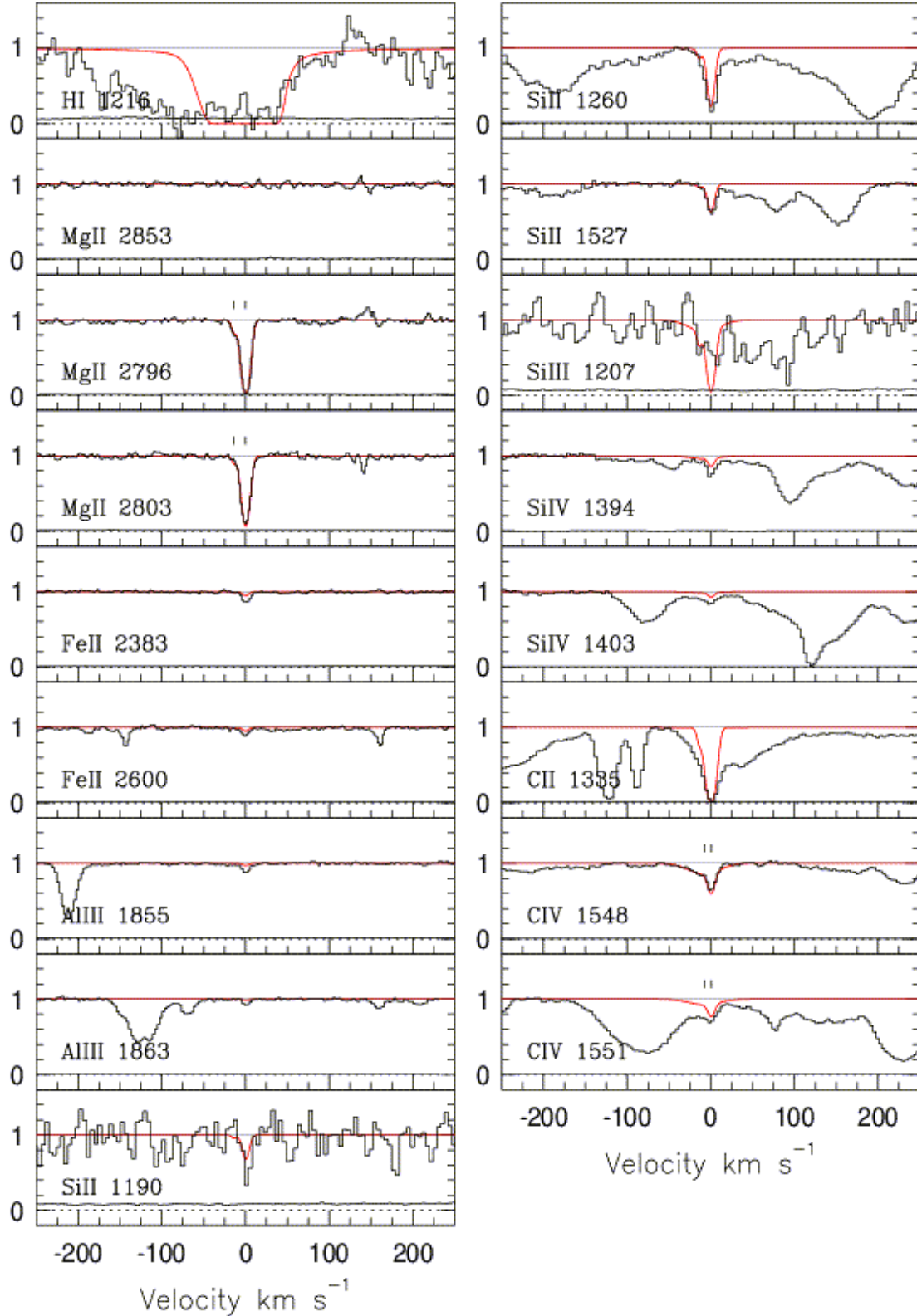


Fig. 7.— The $z = 1.796237$ system towards HE2347-4342, displayed as in Fig. 1. Only relevant transitions are displayed here. This model uses $\log U = -4.0$ for the low ionization phase and $\log U = -2.0$ for the high ionization phase. As explained in §3.7, a second phase is not definitely

Q 0453–423 $z=1.858380$

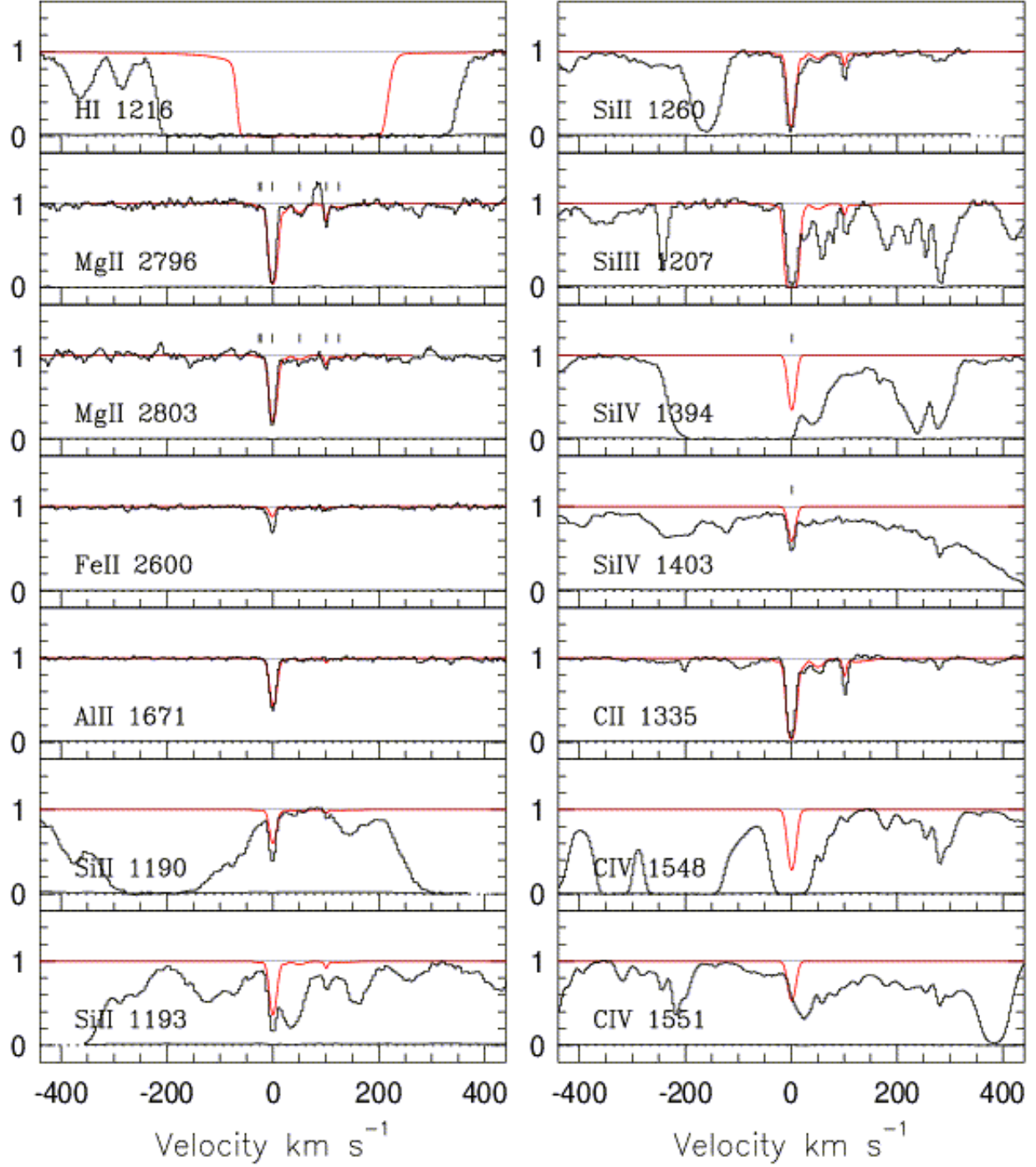


Fig. 8.— The $z = 1.858380$ system towards Q0453-423, displayed as in Fig. 1. Only relevant transitions are displayed here. This model uses $\log U = -4.0$ for the low ionization phase. Here we also use a high ionization phase with $\log U = -2.8$. Metallicity is $\log Z/Z_{\odot} = -1.3$

HE 0940–1050 $z=2.174546$

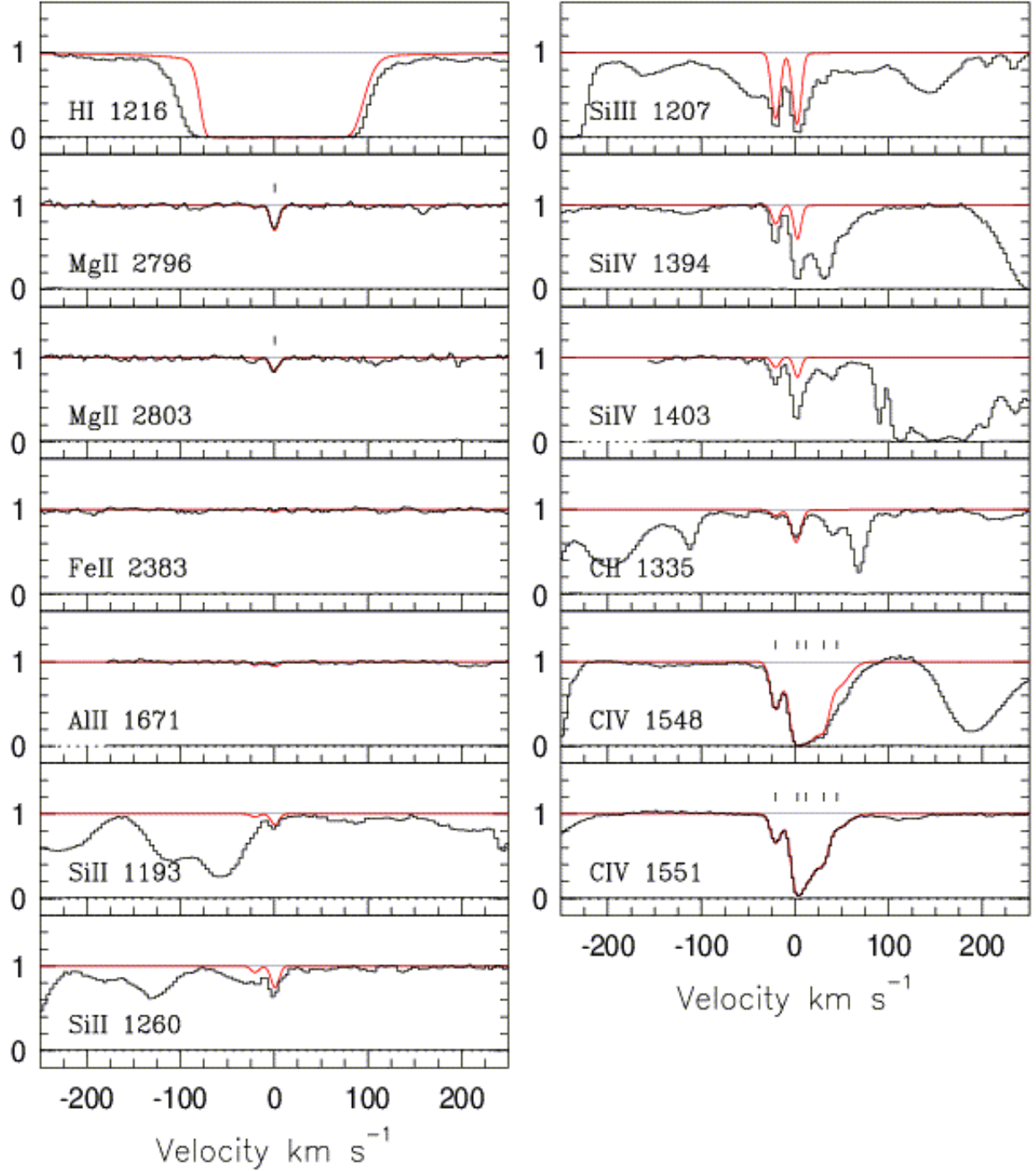


Fig. 9.— The $z = 2.174546$ system towards HE0940-1050, displayed as in Fig. 1. Only relevant transitions are displayed here. This model uses $\log U = -3.7$ for the low ionization phase and $\log U = -2.0$ for the high ionization phase. Metallicity is $\log Z/Z_{\odot} = -2.0$

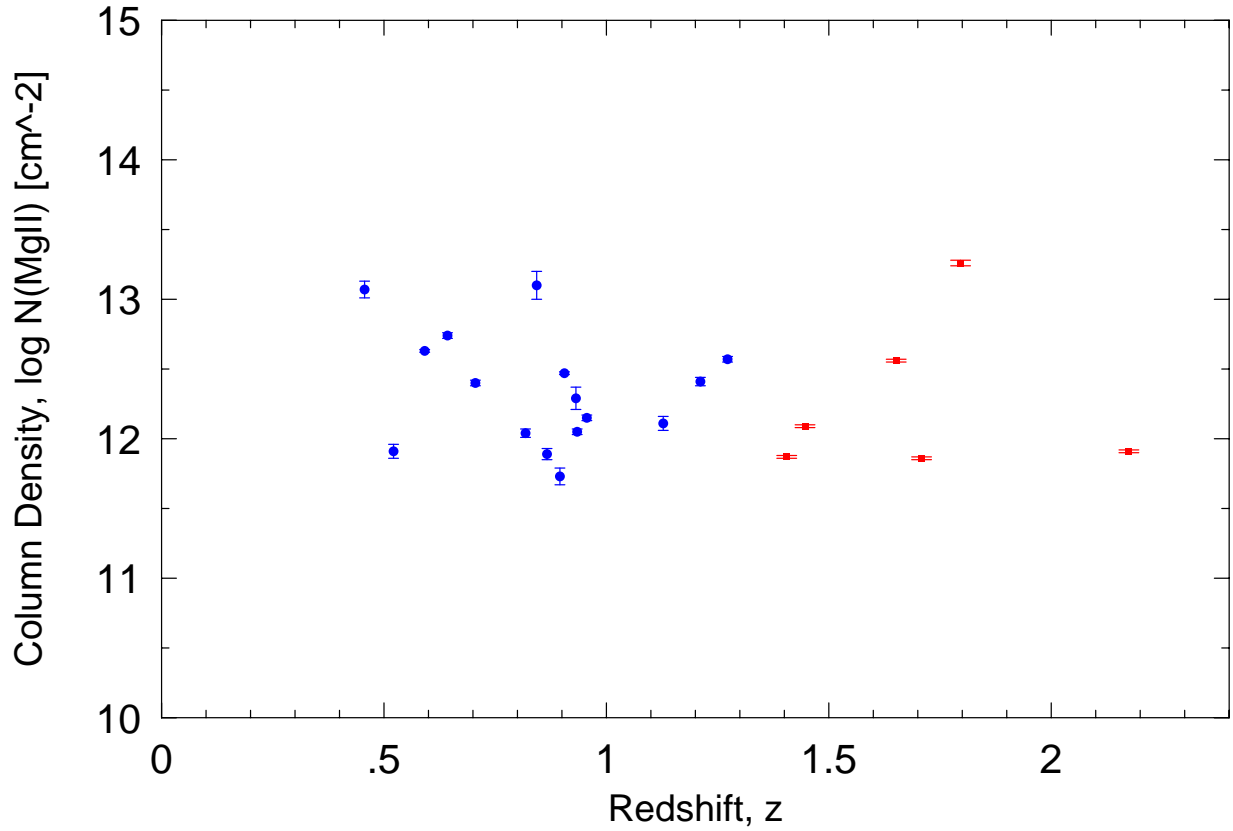


Fig. 10.— Column density vs. redshift for single cloudy weak MgII absorbers. Systems below $z = 1.4$ (circles) were taken from Rigby et al. (2002); Zonak et al. (2004); Ding et al. (2005); Masiero et al. (2005), while systems above $z = 1.4$ (squares) were taken from Lynch et al. (2006). There is no statistical difference between the two populations, giving credence to the theory that the same physical processes have been responsible for the formation of weak MgII absorbers (namely star formation activity in dwarfs) across the given redshift range.

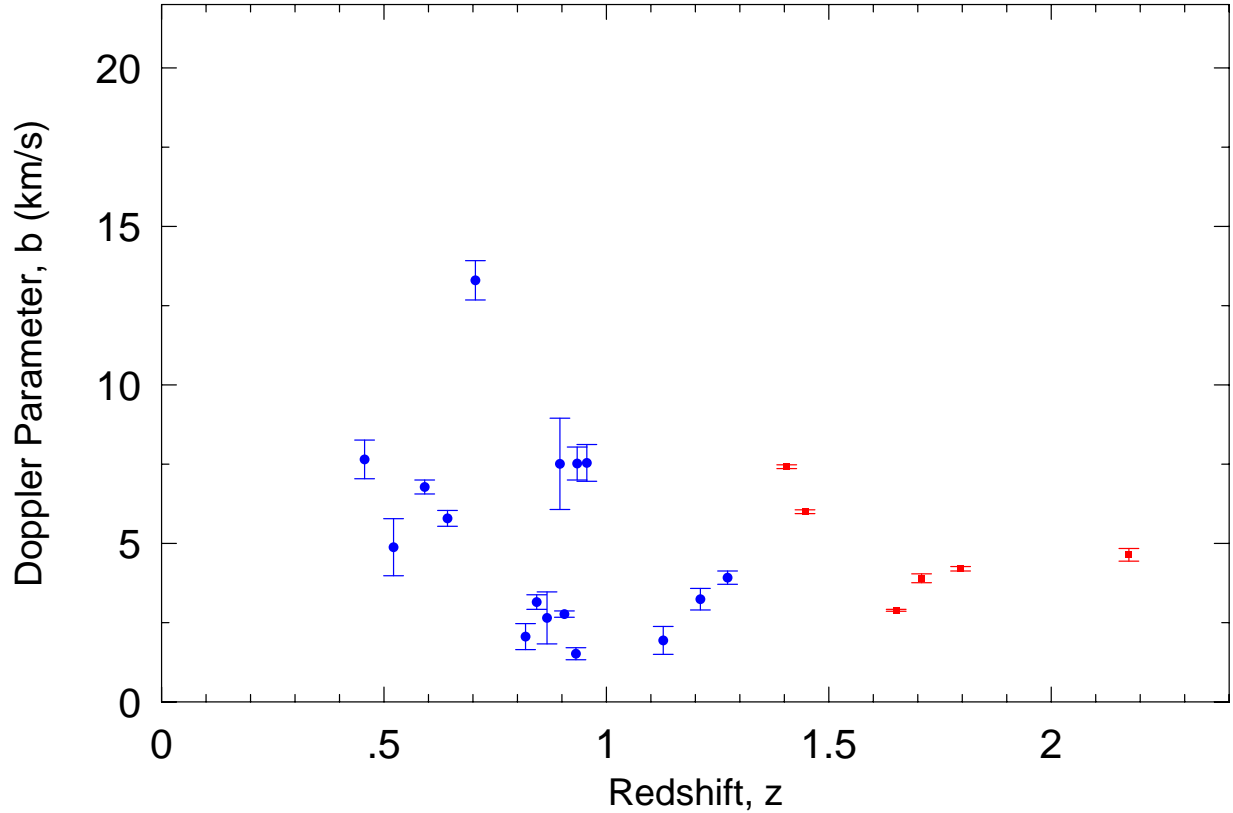


Fig. 11.— Doppler parameter vs. redshift for single cloudy weak MgII absorbers. Systems below $z = 1.4$ (circles) were taken from Rigby et al. (2002); Zonak et al. (2004); Ding et al. (2005); Masiero et al. (2005), while systems above $z = 1.4$ (squares) were taken from Lynch et al. (2006). There is no statistical difference between the two populations, giving credence to the theory that the same physical processes have been responsible for the formation of weak MgII absorbers (namely star formation activity in dwarfs) across the given redshift range.

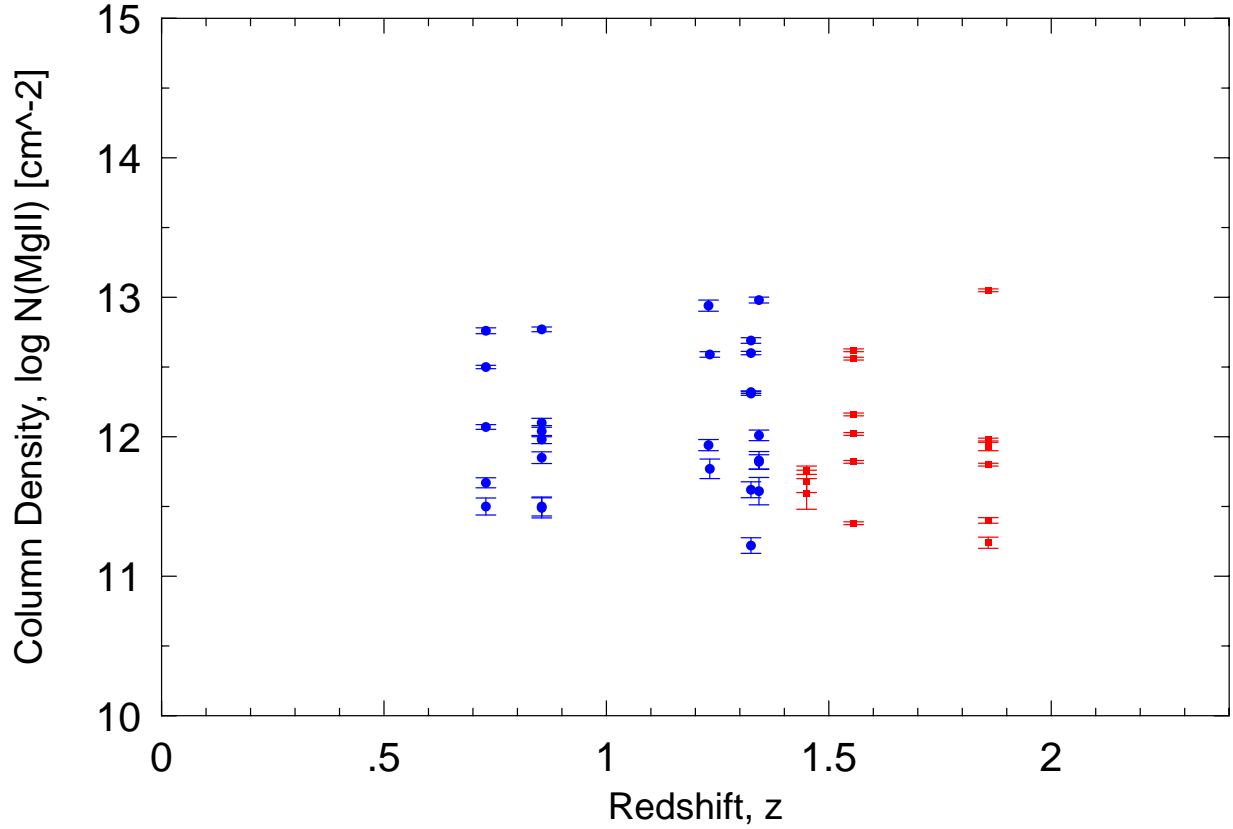


Fig. 12.— Column density vs. redshift for multiple cloudy weak MgII absorbers. Systems below $z = 1.4$ (circles) were taken from Rigby et al. (2002); Zonak et al. (2004); Ding et al. (2005); Masiero et al. (2005), while systems above $z = 1.4$ (squares) were taken from Lynch et al. (2006). There is no statistical difference between the two populations, giving credence to the theory that the same physical processes have been responsible for the formation of weak MgII absorbers (namely star formation activity in dwarfs) across the given redshift range.

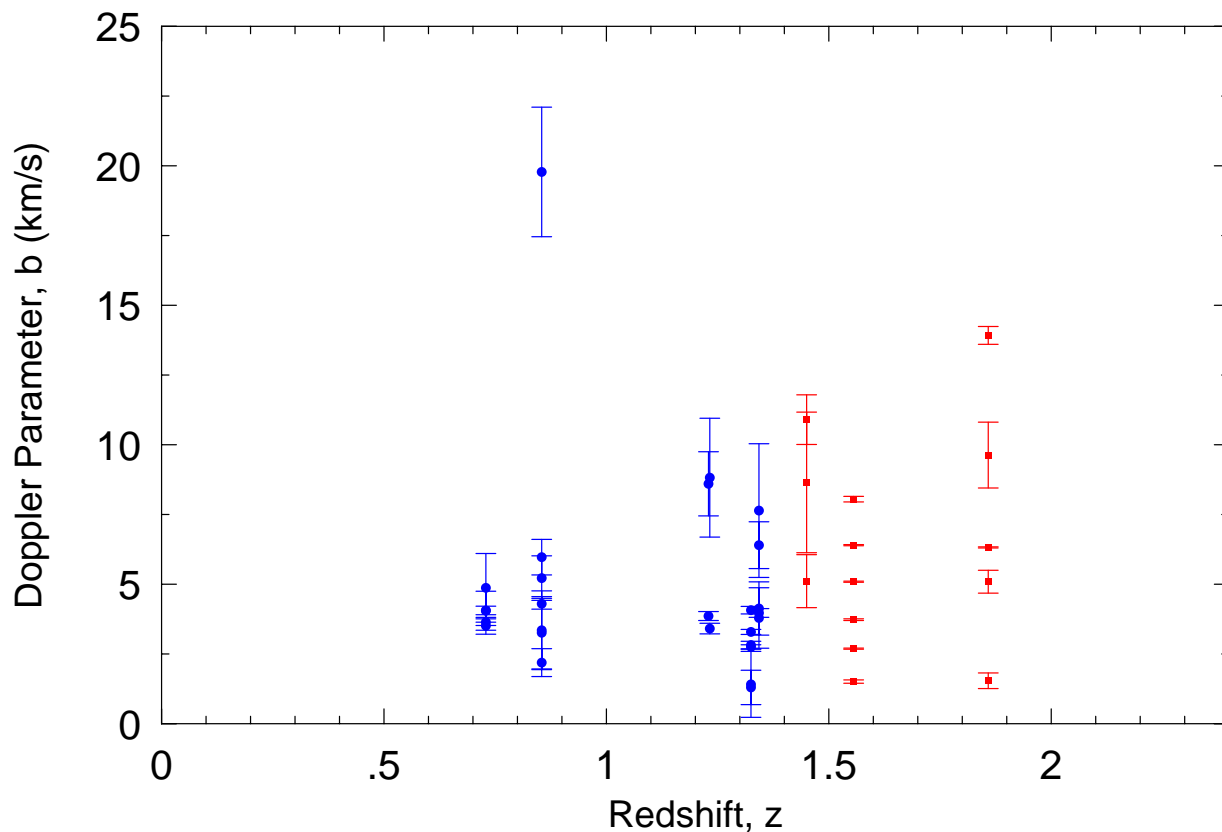


Fig. 13.— Doppler parameter vs. redshift for multiple cloudy weak MgII absorbers. Systems below $z = 1.4$ (circles) were taken from Rigby et al. (2002); Zonak et al. (2004); Ding et al. (2005); Masiero et al. (2005), while systems above $z = 1.4$ (squares) were taken from Lynch et al. (2006). There is no statistical difference between the two populations, giving credence to the theory that the same physical processes have been responsible for the formation of weak MgII absorbers (namely star formation activity in dwarfs) across the given redshift range.

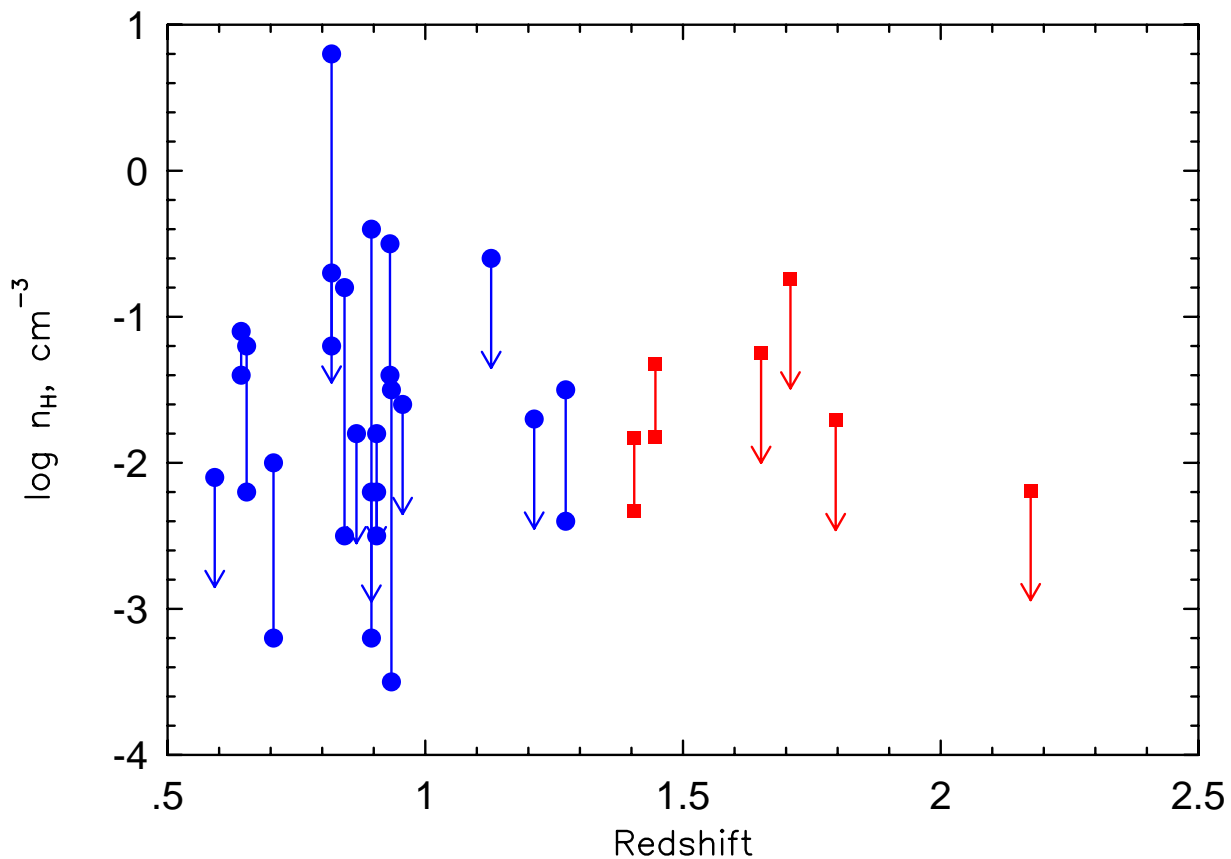


Fig. 14.— Density vs. redshift for single cloudy weak MgII absorbers. Systems below $z = 1.4$ (circles) were taken from Rigby et al. (2002); Charlton et al. (2003); Ding et al. (2005), while systems above $z = 1.4$ (squares) were taken from Lynch et al. (2006). There is no statistical difference between the two populations, giving credence to the theory that the same physical processes have been responsible for the formation of weak MgII absorbers (namely star formation activity in dwarfs) across the given redshift range.

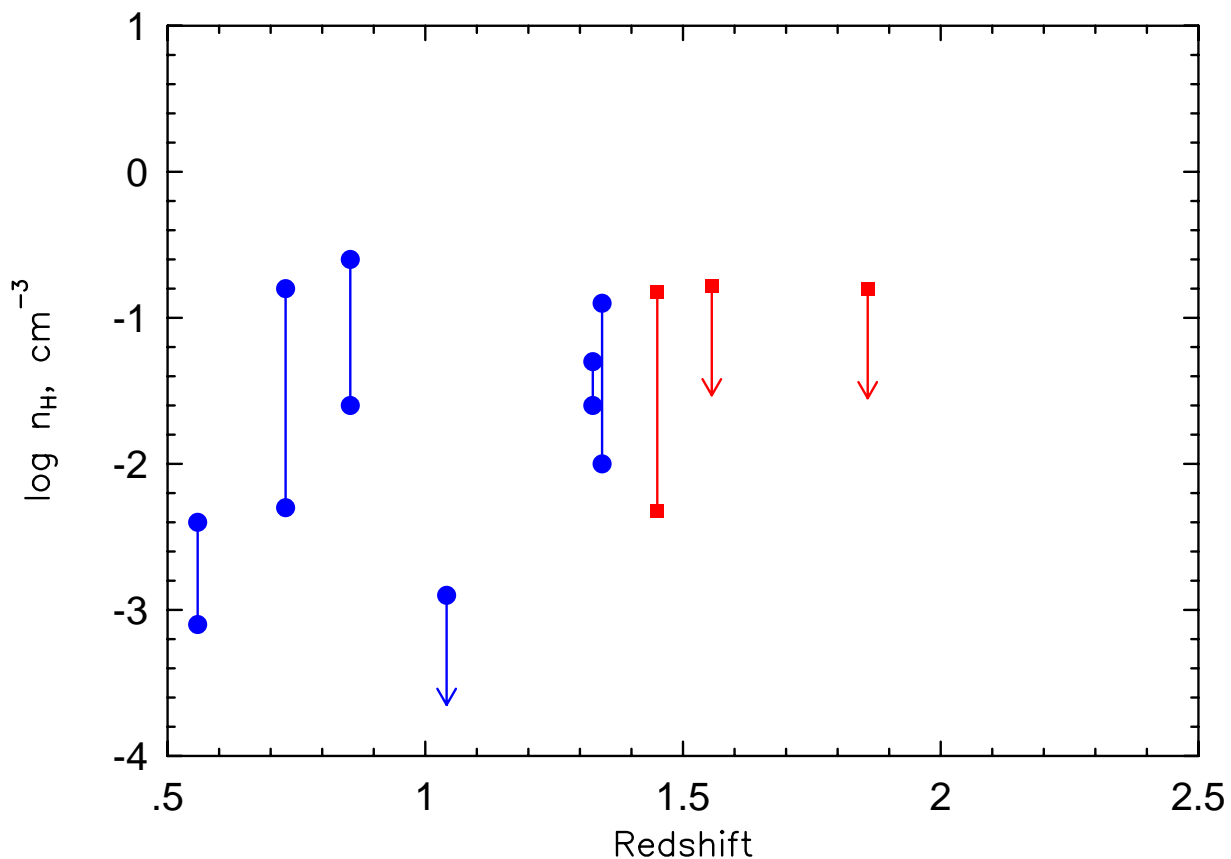


Fig. 15.— Density vs. redshift for multiple cloudy weak MgII absorbers. Systems below $z = 1.4$ (circles) were taken from Rigby et al. (2002); Zonak et al. (2004); Ding et al. (2005); Masiero et al. (2005), while systems above $z = 1.4$ (squares) were taken from Lynch et al. (2006). There is no statistical difference between the two populations, giving credence to the theory that the same physical processes have been responsible for the formation of weak MgII absorbers (namely star formation activity in dwarfs) across the given redshift range.

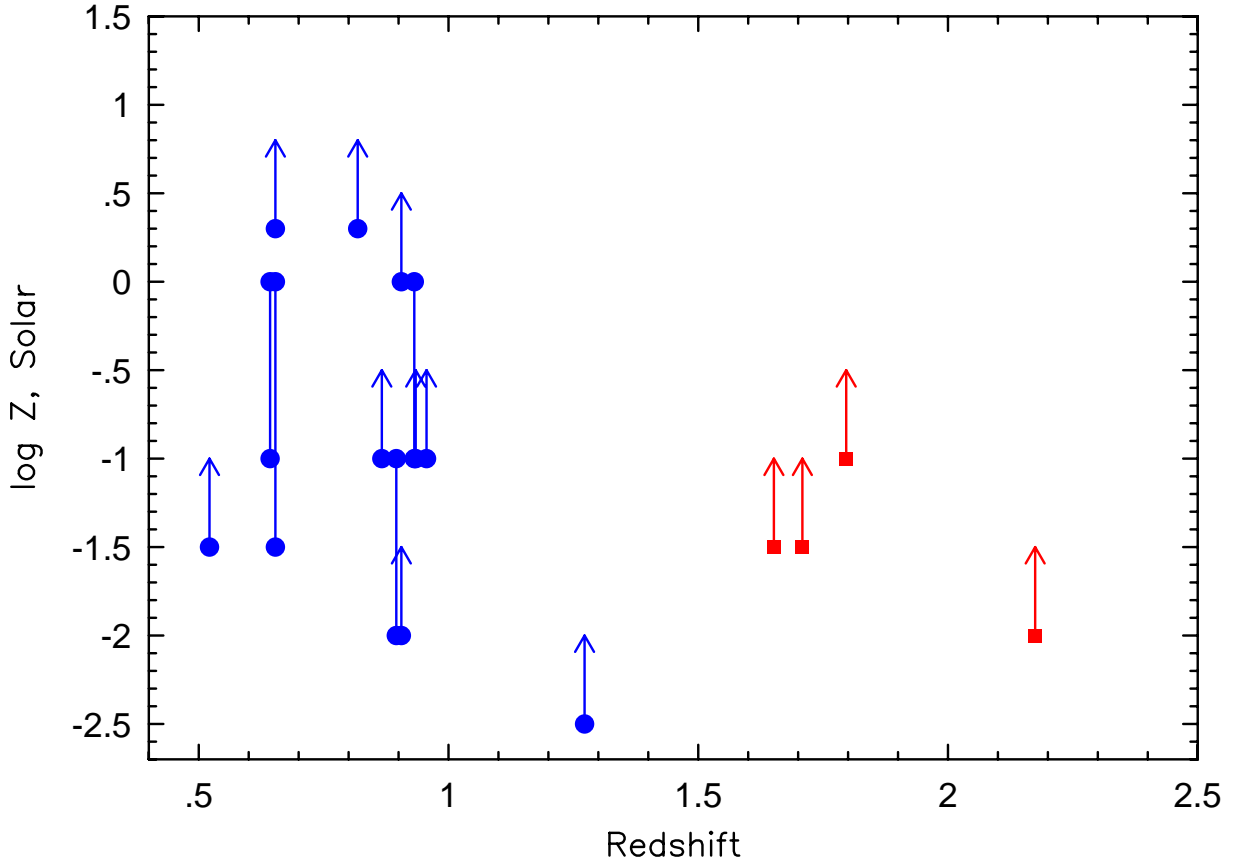


Fig. 16.— Metallicity vs. redshift for single cloudy weak MgII absorbers. Systems below $z = 1.4$ (circles) were taken from Rigby et al. (2002); Charlton et al. (2003); Ding et al. (2005), while systems above $z = 1.4$ (squares) were taken from Lynch et al. (2006). There is no statistical difference between the two populations, giving credence to the theory that the same physical processes have been responsible for the formation of weak MgII absorbers (namely star formation activity in dwarfs) across the given redshift range.

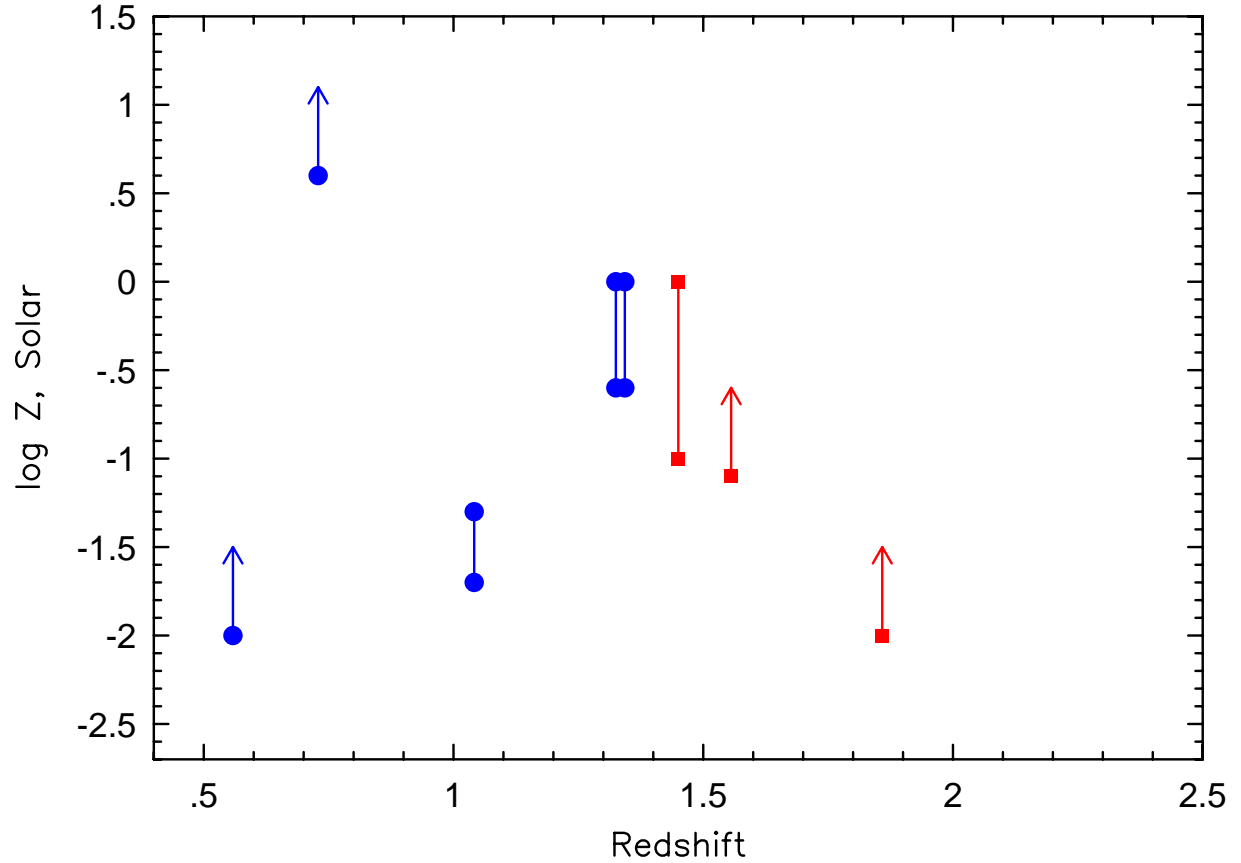


Fig. 17.— Metallicity vs. redshift for multiple cloudy weak MgII absorbers. Systems below $z = 1.4$ (circles) were taken from Rigby et al. (2002); Zonak et al. (2004); Ding et al. (2005); Masiero et al. (2005), while systems above $z = 1.4$ (squares) were taken from Lynch et al. (2006). There is no statistical difference between the two populations, giving credence to the theory that the same physical processes have been responsible for the formation of weak MgII absorbers (namely star formation activity in dwarfs) across the given redshift range.